

Doctoral Thesis (Abridged)

博士論文（要約）

A Simple Calculation Method for Turbine Blade

Load in Shear Flow

（せん断流中におけるタービンブレード荷重の
簡易推定法）

XIA Yiqing

夏 一青

Doctoral Thesis (Abridged)

博士論文（要約）

A Simple Calculation Method for Turbine Blade

Load in Shear Flow

(せん断流中におけるタービンブレード荷重の
簡易推定法)

XIA Yiqing

夏 一青

Dept. of Ocean Technology, Policy and Environment

The University of Tokyo

Nomenclature

A	swept area of the turbine (m^2)
A_L	term in the stall model of Viterna and Corriganis
A_D	term in the stall model of Viterna and Corriganis
A_s	section area (m^2)
A_{sd}	section area at the disk (m^2)
A_{sw}	section area in the far wake (m^2)
$A_{s\infty}$	far upstream section area (m^2)
A_r	aspect ratio
a	axial induction factor
a_c	term in high induction factor correction
a_g	term in empirical solidity equation by Rose
a'	tangential induction factor
B	number of blades
c	blade chord (m)
$c_{0.7}$	chord length at 70 percent radius (m)
$c_{0.75}$	chord length at 75 percent radius (m)
C_P	power coefficient
C_{PF}	power coefficient without blockage effect
C_{PT}	power coefficient with blockage effect
C_{TF}	thrust coefficient without blockage effect
C_{TT}	thrust coefficient with blockage effect
C_D	drag coefficient
$C_{D,s}$	drag coefficient at stall
$C_{D,max}$	maximum drag coefficient
C_L	lift coefficient
$C_{L,s}$	lift coefficient at stall
C_T	thrust coefficient
C_{my}	non-dimensional flapwise bending moment coefficient
C_{my_a}	amplitude of flapwise bending moment coefficient
C_{my_m}	averaged flapwise bending moment coefficient
D	drag force (N)
F	combined loss correction factor

F_{tip}	tip loss factor
F_{hub}	hub loss factor
f_{tip}	term in tip loss correction
dT_1	annular thrust in momentum theory
dT_2	annular thrust in blade element theory
dQ_1	annular torque in the momentum theory
dQ_2	annular torque in blade element theory
g_L	$(dT_1 - dT_2)^2 + (dQ_1 - dQ_2)^2$
h_g	total height of the grid (m)
I	moment of inertia of the rod in the grid (m ⁴)
K	reduced frequency
K_0	term in empirical solidity equation by Rose
L	lift force (N)
L_a	diameter of full scale ocean current turbine blade (m)
L_m	diameter of experiment model turbine blade (m)
M_x	in-plane bending moment at the blade root (N*m)
M_y	out of plane bending moment at the blade root (N*m)
n	turbine rotational rate
P	total kinetic power (W)
Q	rotor torque (N*m)
R	radius of the turbine rotor (m)
Re_{XFoil}	Reynolds number used in XFOil
R_{hu}	radius of the turbine hub (m)
S	distance between rods in the grid (mm)
r	local blade radius (m)
T	rotor thrust (N)
TI	turbulence intensity
T_{max}	maximum thrust of the turbine (N)
TSR	tip speed ratio
TSR_F	tip speed ratio without blockage effect
TSR_T	tip speed ratio with blockage effect
U_0	freestream flow speed at turbine hub center (m/s)
U_T	tunnel speed or test tank carriage speed (m/s)

U_F	free stream speed or test tank carriage speed (m/s)
U	flow velocity (m/s)
U_d	flow velocity at the disk (m/s)
U_w	flow velocity in the far wake (m/s)
U_∞	upstream flow velocity (m/s)
V	fluid velocity (m/s)
V_a	rated velocity of full scale ocean current turbine (m/s)
V_m	velocity of the experimental flow (m/s)
V_{max}	maximum flow velocity (m/s)
W	relative fluid velocity (m/s)
α	attack angle
α_s	stall angle
β	geometrical twisting angle
λ	shear gradient
θ	inflow angle
θ_p	pitch angle of the rotor
$\theta_{c_{my}}$	phase angle of flapwise bending moment coefficient
ρ	fluid density (kg/m ³)
Ω	angular velocity of rotor (rad/s)
σ_r	local blade solidity
σ	solidity
ω_o	oscillating frequency of attack angle

Table of Contents

1. Introduction	1
1.1 Marine Renewable Energy	1
1.1.1 Wind Turbine	2
1.1.2 Tidal Turbine	4
1.1.3 Ocean Current Turbine	9
1.1.4 State of the Art in Japan	12
1.2 Characteristics of Ocean Current Turbines	14
1.2.1 Difference between Ocean Current Turbines and Other Turbines	14
1.2.2 Shear Flow in Ocean Current	17
1.3 Challenges in Ocean Current Turbines	20
1.3.1 Thrust	20
1.3.2 Aspect Ratio	21
1.3.3 Solidity	22
1.4 Literature Review	25
1.4.1 Previous Research Works	25
1.4.2 Numerical Study on Turbine Unsteady Loads	29
1.4.2.1 Dynamic Inflow Model	29
1.4.2.2 Vortex wake model	30
1.4.2.3 Unsteady Model on Blade Section	30
1.4.3 Experimental Investigations on Turbine Unsteady Loads	33
1.5 Purpose of the study	35
1.6 Thesis Outline	37
2. BEM Theory for Ocean Current Turbine Design	38
2.1 BEM Theory	38
2.1.1 Momentum Theory	38
2.1.2 Induction Factor Calculation	40
2.1.3 Limitation of classical BEM Theory	46
2.1.4 Tip Loss Correction	47
2.1.5 Hub Loss Correction	48
2.1.6 High Induction Factor Correction	49
2.2 Blade Element Coefficients	51
2.3 Comparison with Experiments of other Scholars	54

3. Experiment and Comparison with the Classical BEM	56
3.1 Shear Flow Generation	56
3.2 Model Turbine Test and Measurement	59
3.3 Comparison with Classical BEM Model	61
3.3.1 Performance Comparison	61
3.3.2 Bending Moment Comparison	64
4. Unsteady Theory	66
4.1 Unsteady Airfoil Theory	66
4.1.1 Reduced Frequency	68
4.1.2 Attack Angle in Shear Flow	69
4.1.3 Theodorsen's Function	72
4.1.3.1 Boundary Conditions	75
4.1.3.2 Simplifications	75
4.1.3.3 Non-circulatory Forces	79
4.1.3.4 Circulatory Forces	81
4.1.3.5 Kutta Condition	84
4.2 Comparison of Performance	87
4.3 Comparison of Bending Moments	90
5. Discussion	94
5.1 Effect of Tip Speed Ratio on Calculation	95
5.1.1 Effect of Tip Speed Ratio on Attack Angle	95
5.1.2 Effect of Tip Speed Ratio on Induction Factors	98
5.1.3 Effect of Tip Speed Ratio on Power Coefficient	103
5.2 Effect of Pitch Angle on Calculation	107
5.3 Effect of Tip Loss and Hub Loss Correction	112
5.3.1 Tip Loss Factors and Hub Loss Factors	113
5.3.2 Effect of Tip Speed Ratio on Induction Factors	118
5.4 Effect of Drag Coefficient	123
5.5 Comparison of Theodorsen's Function with Loewy's Function	129
5.6 Comparison with CFD Results in High Shear Gradient	133
6. Summary and Conclusion	138
6.1 BEM Model	138
6.2 Unsteady Airfoil Theory	139

6.3 Important Parameters in Turbine Design	140
Acknowledgement	143
Reference	144
Appendix	153
A.1 Shear Flow Generation	153
A.1.1 Froude Similarity	154
A.1.2 Shear Flow Generator Grid Design	154
A.1.3 Shear Flow Generator Grid Design	156
A.1.4 Flow Measurement	157
A.2 Model Turbine Test in the Circulating Water Channel	160
A.3 Model Turbine Test in the Towing Tank	165
A.4 Analysis of Experimental Data	168
A.4.1 Blockage Correction	168
A.4.2 Analysis of Experimental Data in Frequency Domain	169
A.4.3 Analysis of Experimental Data in Time Domain	171
A.5 Limitation of Experiments	174
A.6 Experiments of Ocean Current Turbine Model	175
A.6.1 Turbine Tests in the Circulating Water Channel in Akishima Laboratories Inc	175
A.6.2 Turbine Tests in the Towing Tank	178

Table of Figures

Fig 1.1 Progression of expected wind turbine evolution to deeper water	3
Fig.1.2 Major ocean surface currents	11
Fig 1.3 Concept of ocean current turbines in Japan	12
Fig 1.4 Verification test of the ocean current turbine off Kuchinoshima	13
Fig 1.5 A 1MW tidal turbine against a 1MW wind turbine	15
Fig 1.6 The Kuroshio Current path	17
Fig 1.7 One hour averaged current speed in March 13, 2013	18
Fig 1.8 Averaged current speed for the period: March 13, 2013 – June 30, 2013	18
Fig 1.9 Expected performances of different types of turbines	23
Fig 1.10 Decomposition of forcing into perturbations to local attack angle and velocity field	31
Fig 2.1 Actuator disc and stream tube concept	39
Fig 2.2 Forces and velocities on a blade section	41
Fig 2.3 Flow chart of induction factor calculation	45
Fig 2.4 Different expressions for the thrust coefficient C_T with the axial induction factor a	50
Fig 2.5 2-D lift coefficient data of NACA0012 airfoil	52
Fig 2.6 2-D drag coefficient data of NACA0012 airfoil	53
Fig 2.7 Comparison of Power Coefficient- TSR curve with Bahaj's experiment	54
Fig 2.8 Comparison of Thrust coefficient- TSR curve with Bahaj's experiment	55
Fig 3.1 Shear flow profile with water depth generated by the three screen system	57
Fig 3.2 Shear flow profile with water depth generated by the three screen system in the circular water channel of Akishima Laboratories Inc.	58
Fig 3.3 Side and front view of experimental turbine	59
Fig 3.4a Comparison of power coefficients with TSR when pitch angle is -2°	61
Fig 3.4b Comparison of thrust coefficients with TSR when pitch angle is -2°	62
Fig 3.5a Comparison of power coefficients with TSR when pitch angle is 0°	62
Fig 3.5b Comparison of thrust coefficients with TSR when pitch angle is 0°	63
Fig 3.6a Comparison of averaged flapwise bending moment coefficients when pitch angle is -2°	64
Fig 3.6b Comparison of averaged flapwise bending moment coefficients when pitch angle is 0°	65

Fig 4.1a Force and moment on an airfoil by classical BEM theory	66
Fig 4.1b Combination of BEM and unsteady airfoil theory on an airfoil	66
Fig 4.1c Model of a blade element of ocean current turbine in Theodorsen's function	67
Fig 4.2 Reduced frequency distribution with tip speed ratios at $C_{0.2R}$	68
Fig 4.3 Forces and velocities on a blade section	69
Fig 4.4 Time history of attack angle for a blade element with $r/R=0.5$, pitch angle -2 degree	72
Fig 4.5 Time history of relative flow speed for a blade element with $r/R=0.5$, pitch angle -2 degree	73
Fig 4.6 Model of a blade element of ocean current turbine	74
Fig 4.7 Joukowski's conformal transformation	77
Fig 4.8 Singularities of the Theodorsen Function	77
Fig 4.9 Wing and wake of the Theodorsen Function	78
Fig 4.10 Vortex distribution in Theodorsen's function	81
Fig 4.11 Comparison of Jone's approximation with Theodorsen's coefficient C_k for a variation of the reduced frequency	86
Fig 4.12a Comparison of power coefficients with TSR when pitch angle is -2°	87
Fig 4.12b Comparison of thrust coefficients with TSR when pitch angle is -2°	88
Fig 4.13a Comparison of power coefficients with TSR when pitch angle is 0°	88
Fig 4.13b Comparison of thrust coefficients with TSR when pitch angle is 0°	89
Fig 4.14a Comparison of C_{my} amplitude when pitch angle is -2°	90
Fig 4.14b Comparison of C_{my} amplitude when pitch angle is 0°	91
Fig 4.14c Comparison of C_{my} amplitude when pitch angle is 2°	91
Fig 4.15a Comparison of C_{my} phase shift when pitch angle is -2°	92
Fig 4.15b Comparison of C_{my} phase shift when pitch angle is 0°	92
Fig 4.15c Comparison of C_{my} phase shift when pitch angle is 2°	93
Fig 5.1a Distribution of attack angle with radius when pitch angle is -2°	96
Fig 5.1b Distribution of attack angle with radius when pitch angle is 0°	96
Fig 5.1c Distribution of attack angle with radius when pitch angle is 2°	97
Fig 5.2a Distribution of induction factor with radius when pitch angle is -2°	99
Fig 5.2b Distribution of induction factor with radius when pitch angle is 0°	99
Fig 5.2c Distribution of induction factor with radius when pitch angle is 2°	100
Fig 5.3a Distribution of tangential induction factor with radius when pitch angle is -	

2°	101
Fig 5.3b Distribution of tangential induction factor with radius when pitch angle is 0°	101
Fig.5.3c Distribution of tangential induction factor with radius when pitch angle is 2°	102
Fig 5.4 Comparison of Power Coefficient- <i>TSR</i> curve with Bahaj's experiment	103
Fig 5.5 Comparison of Thrust coefficient- <i>TSR</i> curve with Bahaj's experiment	103
Fig 5.6 Comparison of power coefficients with <i>TSR</i> when pitch angle is 0°	104
Fig 5.7 Comparison of thrust coefficients with <i>TSR</i> when pitch angle is 0°	104
Fig 5.8 Attack distribution of Bahaj's model when <i>TSR</i> is 3	106
Fig 5.9 Attack distribution of Bahaj's model when <i>TSR</i> is 4	106
Fig 5.10 Distribution of induction factor with radius when <i>TSR</i> is 4	108
Fig 5.11 Distribution of induction factor with radius when <i>TSR</i> is 7	108
Fig 5.12 Distribution of induction factor with radius when <i>TSR</i> is 11	109
Fig 5.13 Distribution of induction factor with radius when <i>TSR</i> is 4	110
Fig 5.14 Distribution of induction factor with radius when <i>TSR</i> is 7	110
Fig 5.15 Distribution of induction factor with radius when <i>TSR</i> is 11	111
Fig 5.16 Distribution of tip loss factor with radius when <i>TSR</i> is 4	113
Fig 5.17 Distribution of tip loss factor with radius when <i>TSR</i> is 7	114
Fig 5.18 Distribution of tip loss factor with radius when <i>TSR</i> is 11	114
Fig 5.19 Distribution of hub loss factor with radius when <i>TSR</i> is 4	115
Fig 5.20 Distribution of hub loss factor with radius when <i>TSR</i> is 7	115
Fig 5.21 Distribution of hub loss factor with radius when <i>TSR</i> is 11	116
Fig 5.22 Distribution of combined loss factor with radius when <i>TSR</i> is 4	116
Fig 5.23 Distribution of combined loss factor with radius when <i>TSR</i> is 7	117
Fig 5.24 Distribution of combined loss factor with radius when <i>TSR</i> is 11	117
Fig 5.25 Distribution of attack angle with radius when <i>TSR</i> is 4	119
Fig 5.26 Distribution of attack angle with radius when <i>TSR</i> is 7	119
Fig 5.27 Distribution of attack angle with radius when <i>TSR</i> is 11	120
Fig 5.28 Distribution of induction factor with radius when <i>TSR</i> is 7	120
Fig 5.29 Distribution of induction factor with radius when <i>TSR</i> is 11	121
Fig 5.30 Distribution of tangential induction factor with radius when <i>TSR</i> is 4	121
Fig 5.31 Distribution of tangential induction factor with radius when <i>TSR</i> is 7	122

Fig 5.32 Distribution of tangential induction factor with radius when TSR is 11	122
Fig 5.33 NACA0012 lift coefficients based on measured data by Burton et al.	124
Fig 5.34 NACA0012 drag coefficients based on measured data by Burton et al.	125
Fig 5.35a Comparison of power coefficients with TSR when pitch angle is -2°	126
Fig 5.35b Comparison of thrust coefficients with TSR when pitch angle is -2°	126
Fig 5.36a Comparison of power coefficients with TSR when pitch angle is 0°	127
Fig 5.36b Comparison of thrust coefficient- TSR curve when pitch angle is 0°	127
Fig 5.37 Comparison of Power coefficient- TSR curve when pitch angle is 10°	128
Fig 5.38 Model of a thin airfoil in harmonic oscillation by Theodorsen	129
Fig 5.39 Model of airfoil oscillation by Loewy	130
Fig 5.40 Comparison of Theodorsen's function with Loewy's function in amplitude of C_{my}	131
Fig 5.41a Comparison of time histories of the nondimensional power with CFD results for $TSR=7$	133
Fig 5.41b Comparison of time histories of nondimensionalized thrust with CFD results for $TSR=7$	134
Fig 5.42 Comparison of time histories of nondimensional flapwise bending moment with CFD results for $TSR=7$	134
Fig 5.43a Local averaged attack angle distribution when $TSR=5$, shear flow with shear gradient 40%	136
Fig 5.43b Local averaged attack angle distribution when $TSR=5$, shear flow with shear gradient 10%	136
Fig 5.44a Local averaged attack angle distribution when $TSR=7$, shear flow with shear gradient 40%	137
Fig 5.44b Local averaged attack angle distribution when $TSR=7$, shear flow with shear gradient 10%	137
Fig A.1 Scene graph of the circulating water channel in Chiba station	153
Fig A.2 Grid solidity distribution	154
Fig A.3 Arrangement of the grid and coordinate system	156
Fig A.4 Front view of the non-uniform grid	156
Fig A.5 Arrangement of electromagnetic current meters	158
Fig A.6 Schematic diagram of the turbine testing experiment	158
Fig A.7 Measured flow velocity with water depth	159

Fig A.8 Internal layout of experimental turbine	161
Fig A.9 Side and front view of experimental turbine	161
Fig A.10 1/50 scale model of two bladed horizontal axis ocean current turbine.....	162
Fig A.11 Starting position of the phase angle	164
Fig A.12 Model turbine in the circulating water channel at 0.48 m/s	164
Fig A.13 Model turbine in the towing tank	166
Fig A.14 Schematic diagram of the experimental arrangement in the towing tank	166
Fig A.15 Blockage corrections for 1° pitch angle	168
Fig A.16a Power spectrum of the out-of-plane bending moment at the blade root when pitch angle is 1°	169
Fig A.16b Power spectrum of the angular velocity when pitch angle is 1°.....	170
Fig A.17a Measured time history of angular velocity of the ocean current turbine rotor with target <i>TSR</i> of 9.1	171
Fig A.17b Measured time history of angular velocity of the ocean current turbine rotor with target <i>TSR</i> of 6.4	172
Fig A.18a Measured time histories of loads in the shear flow with target <i>TSR</i> of 9.1 ·	173
Fig A.18b Measured time histories of loads in the shear flow with target <i>TSR</i> of 6.4 ·	173
Fig A.19 Measured flow speed with water depth in Akishima Laboratories Inc	175
Fig A.20 Side view of the test turbine in the shear flow.....	176
Fig A.21 Photograph of the test turbine in the towing tank	178

Table of Tables

Table 1.1 Tidal energy extraction devices	6
Table 3.1 Size parameters of the circulating water tank	57
Table 5.1 Comparison of amplitude of C_{my} in different $TSRs$ with CFD results	135
Table A.1 Size parameters of the circulating water tank	153
Table A.2 Deflection and drag force under different grid diameters	157
Table A.3 Geometry of turbine blades and hub	163
Table A.4 Blockage corrections for 0° pitch angle at $TSR=8$	168
Table A.5 Geometry of turbine blades tested in Akishima Laboratories Inc.	177

1 . Introduction

1.1 Marine Renewable Energy

Nowadays, the greenhouse effect has drawn increasing attention under the background of human beings coping with climate change. With efforts to reduce greenhouse gas emission, the depletion of traditional fossil energy resources, such as coal and oil, drivers of climate change, is another challenge faced by human society. Countries around the world have formulated strategies for energy transformation, proposed higher energy efficiency targets, and came up with more active low-carbon policies. Especially developed countries are constantly seeking low-cost clean energy alternatives to promote economic green and low-carbon transformation.

The United Nations Climate Change Paris Agreement set new and higher requirements in 2015, clarifying the goal of achieving global greenhouse gas emissions and absorption phase balance in the second half of the 20th century, will drive the energy supply system with new energy and renewable energy as the main body to form as soon as possible [1]. Green cleaning and low carbon is the direction of energy development, which is the consensus of all countries.

In this background, renewable energy, including wind energy, ocean energy, geothermal energy, hydropower, modern biomass and solar energy, has progressed rapidly in recent years. With no doubt that renewable energy over the world will continue to grow rapidly in the future due to the necessity of human beings for sustainable development.

1.1.1 Wind Turbine

The rapid development of the global economy accompanies an increase in the world's energy consumption, hence renewable, green, and clean energy such as wind energy, solar energy, as one of the solutions of energy crisis and greenhouse effect, has become promising. Among a variety of renewable energy, wind energy stands out for low cost and feasibility to make use of. Increasing developers, companies and countries are paying attention to this new, attractive choice to utilize [2].

Compared with the electricity generation by conventional fossils, wind energy has enhanced competitiveness with the development of technology. For the offshore type of wind energy, it has an economic disadvantage on construction and maintenance over wind energy on land. Nevertheless, there are several reasons for adopting offshore wind energy, for example, higher wind resources, less environmental and noise impact, and more available space. The trend has begun that offshore wind farms lately are developing to deep sea [3]. While moving to offshore, it will be costly due to rising difficulty in operation and maintenance of the turbine support structures. For offshore wind farms, there are other additional costs in cabling, transportation, and installation that also need to be considered.

Fixed foundation turbines are adopted by the majority of currently operating offshore wind farms, with a few new projects using floating types. Fixed foundation offshore wind turbines are usually installed in relatively shallow waters less than 50 m deep, with fixed foundations underwater [4]. There are monopile, tripod, and jacket wind turbines with various foundations used as diverse types of underwater structures at the seafloor including monopile or multiple piles, caissons and gravity base [4]. For different water depths, there are a variety of bases adopted by offshore wind turbines for stability.

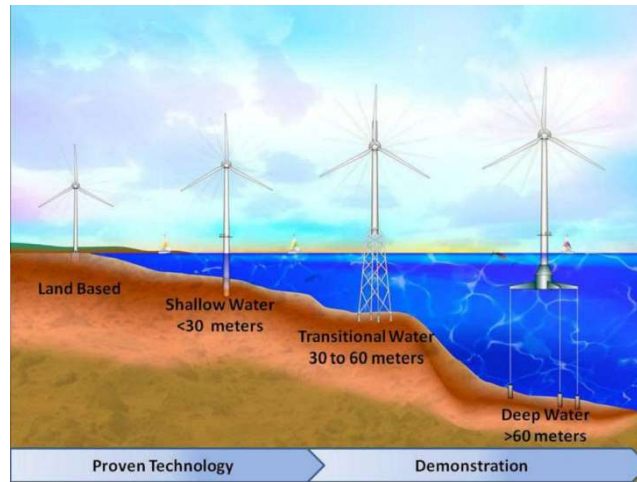


Fig 1.1 Progression of expected wind turbine evolution to deeper water [4]

As seen in Fig 1.1, for locations with depths over sixty to eighty meters, it is difficult and expensive to use fixed foundations, hence floating wind turbine concepts become necessary [5, 6, 7]. Hywind, installed in 2009, is known as the first full-scale floating wind turbine [8]. 2017 has witnessed the first operational large-scale floating offshore wind farm, which is based on that model. There are other floating wind turbine models in test and more are under planning. Most of them are horizontal axis wind turbines. However, offshore vertical axis turbines have also been proposed and studied. The vertical axis wind turbines have advantages such as a low gravity center and easy installation for larger scale than the horizontal axis turbines, which may contribute to the decrease of the capital price of the offshore wind generation [9]. However, the industry hasn't reached the application stage yet for the vertical wind turbines.

1.1.2 Tidal Turbine

The ocean contains a variety of renewable sources. There are many forms, such as offshore wind energy, tidal energy, current energy, wave energy, ocean thermal energy, ocean infiltration energy, and marine biomass energy. The development of ocean renewable resources has grown rapidly in the 21st century [10, 11].

Generally, tides and currents are recognized as two principal forms of ocean energy. Tidal energy is caused by the combination of the earth's rotation and the gravitational interaction between the oceans, the moon, and the sun. Ocean energy also includes ocean swells and wave energy that can be adopted with proper devices.

The tide is the phenomenon of the rise and descent of seawater, which is due to the force between the celestials, such as the sun, the earth, the moon. Spring tide is when the seawater rises to the maximum, and neap tide is when the seawater falls to the lowest level. Along with advances in technology, the use of electric and electronic equipment is rapidly increasing. There is future demand to generate extra capacity other than existing power.

Tidal energy is recognized as one of the best existing renewable sources. Tidal energy has a long-term perspective and can be more accurately predicted compared with wind energy, solar energy, thermal energy and so on. Tidal energy is clean and not exhausted. Because of these features, it is unique and appropriate to use tidal energy as a power generation source in the future. There are variations in the tidal power plants around the world accompanied by different tide levels. Also, the method of converting tidal energy to electrical energy is site-specific. In general, however, the way to extract energy from the tide is similar to a conventional hydropower plant.

There are three types of low tide: diurnal, semidiurnal and mixed [12]. Tidal energy is one of the new and evolving technologies that are still in the Research and Development (R & D)

stage. Tidal energy is inexhaustible and can be thought of as a renewable energy source [13]. Thus one of its advantages is less susceptible to climate change, while other sources are vulnerable to random changes in climate [14]. Review from the Energy Technical Assistance Unit (ETSU) on tidal energy was the first attempt to estimate energy of UK tidal resources [15]. The points marked by ESTU were later investigated and revised in 2001 in documents submitted to the UK Trade and Industry Ministry (DTI) by Binnie, Black, and Veatch. Existing technologies used for tidal energy are generally conversion from wind power generation [16, 17, 18]. Researchers predicted that the UK can produce more than 20% of the electricity demand from tidal resources [19]. There have been researches focusing on availability of tidal energy. However, it is also important to consider the effect of extracting energy using renewable energy sources. It is necessary for developers to understand when and where to stop energy extraction so that disturbance caused by periodic natural phenomena is minimized.




The advantage of tidal energy is that it can be predicted accurately because of astronomical nature. The accuracy rate of prediction has been up to within 98% in decades [10]. Recently, a variety of tidal turbines, including horizontal axis and vertical axis types, have been in the development stage [20, 21, 22]. Ng et al. [23] made a detailed review of tidal turbine hydrodynamic design and tidal turbine farms in the last decade. Horizontal axis turbines account for the majority of the industrialized tidal turbines, since vertical axis turbines generally have defects as strong fluctuations in torque, less power efficiency, low self-starting ability, compared with horizontal axis turbine designs. Ng et al. [23] concluded that presently for large-scale turbines over 500 kW, the horizontal axis tidal turbines are considered to be the best choice in both technology and economy.


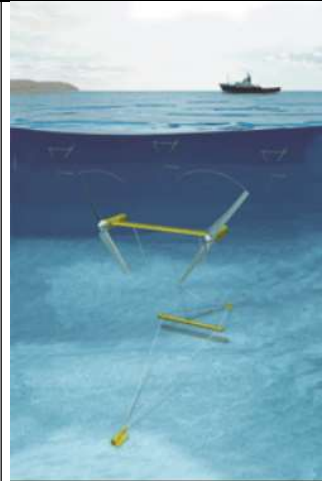


Some projects of tidal turbines have been published in the design phase a few years ago [10, 19]. It can be noticed that some projects, including lunar energy tidal turbines and blue energy tidal turbines, are abandoned without commercialization. There are some tidal turbine models


without more information following the first announcement as well. In addition, in recent years, we have witnessed some turbine concepts changed names and scale.

There are a variety of tidal energy devices used for energy extraction in different sites. The details of some typical models are given in Table 1.1.

Table 1.1 Tidal energy extraction devices

Turbine	Developer	Power Output	Rotor	Diameter [m]	Depth [m]	Horizontal Axis(HA) or Vertical Axis(VA)	
OpenHydro	OpenHydro , Irish	500KW	Multi-blades, two turbines	16	35	HA	 <p>OpenHydro [24]</p>
HS1000	Andritz Hydro Hammerfest, UK	1MW	Three bladed	20	35-100	HA	 <p>HS1000 [25]</p>
Seagen	Marine Current Turbines Ltd. , UK	1.2 MW	Twin two bladed rotor	16		HA	 <p>Seagen [26]</p>

The Blue Concept	Hammerfest Strom, Norway	1 MW	Three bladed			HA	 <p>The Blue Concept [27]</p>
TidEL	SMD Hydrovision of Tyne and Wear, UK	1 MW	Twin two bladed tethered rotor	15		HA	 <p>TidEL [28]</p>
Stingray	Engineering Business Ltd., UK	500 kW	Oscillating Hydroplane				 <p>Stingray [29]</p>
Voith Hydro HyTide turbine	Voith Company, Germany	1 MW	Three bladed	13		HA	 <p>Voith Hydro HyTide turbine [30]</p>

Sabella D10 turbine	Sabella Company, France	1MW	Six bladed	10	55	HA	 <p data-bbox="1155 477 1425 501">Sabella D10 turbine [31]</p>
---------------------	-------------------------	-----	------------	----	----	----	---

Aiming at developing a brand new generation that is economical, efficient, and to extract tidal energy while friendly to the marine environment, the tidal turbine industry has drawn considerable attention. One advantage of tidal turbines is that they are most likely less harmful to environments than those of other sources of electricity generation, but more studies are still necessary at this point. It is of necessity to contemplate the influence of energy extraction, whereas estimating the yield energy from a possible site of tidal energy.

Whether human beings extensively extract the tidal energy in the future will be determined by the electricity capital price compared with other energy, as well as the effect on environments. If the majority of this tidal energy resource can be utilized effectively, with no doubt a major contribution to the energy requirements of human kinds will be made.

1.1.3 Ocean Current Turbine

Another important ocean energy is the ocean current. The main component of the ocean currents can be predicted years in advance by simulations. Additionally, as a highly predictable energy resource, the ocean currents are carried by seawater, a fluid medium 800 times denser than the air, which means it can offer energy output greater than onshore renewable energy [16]. Recently, ocean currents are reported to have the potential to meet the world's energy demand to a large extent [32]. In other words, it is possible to extract significant electrical power from ocean currents.

Japan is an island country that is surrounded by the oceans. It has a huge ocean energy resource potential such as ocean currents, tidal currents and wave power in the exclusive economic zone as a big advantage. Ocean energy generation, which utilizes energy from wave power, ocean current power, and tidal current power, is expected to create new industries and improve Japanese energy security as a new source of renewable energy.

Ocean current energy has an advantage of stability over wave energy, tidal energy, and wind power. However, we have to admit that the ocean current speed is generally slow compared to the tidal current speed which is utilized in Europe and North America. Moreover, the deep sea water depth is over 200m in the Kuroshio Current. In order to realize an ocean current turbine system and achieve the power generation at lowest possible costs, the University of Tokyo, IHI, and Japan's New Energy and Industrial Technology Development Organization (NEDO) have proposed a floating type of ocean current turbine which does not need extra support structures for standing on the seabed, with the capability of easy installation and maintenance. Improvements in efficiency and reliability, as well as other elemental technologies that contribute to the reduction of the cost are under research now.

Ocean current turbine is of great importance to Japan in the ocean energy field. After the oil crisis in the 1970th, Japan had a leading role in the global study and development of ocean

energy until the end of the 20th century. Later on, with significantly fewer countries active in developing ocean energy, Japan also slowed down the pace for the study of ocean energy extraction. Nevertheless, Britain, Portugal, Norway, and other European countries continued their studies on ocean energy. Over the subsequent decade, the energy yields from wave devices and wind turbines expanded over ten times by their work. Steady progress was witnessed by the large-scale advanced devices in operation such as the offshore floating wind turbine Hywind, the tidal turbine SeaGen, and the wave generator Pelamis.

As a giant and stable ocean energy resource, the Kuroshio Current has made Japan more promising in the ocean current energy, over Europe which has advanced technologies for offshore wind and tidal energy. Hence it is of great importance to utilize Kuroshio's energy efficiently for which there is an inherent geographical advantage as a next-generation ocean energy technology. Moreover, the international competitiveness of Japan's marine renewable industries will be potentially improved.

There are complicated patterns in the ocean currents, influenced by quite a few parameters, like wind, water salinity, water temperature, water depth, water refraction, and water diffraction. Wind and solar energy from the sea surface in the tropics are the main driving forces of ocean currents, while in some cases, fluctuation in seawater density and salinity also result in ocean currents. As shown in Fig 1.2, there are several major ocean surface currents all over the world, including Kuroshio Current. Compared with the tide turbines which are usually installed nearshore, ocean currents have stable energy and the flow is generally in one direction. Although the current speed is much slower than wind speed adopted by wind turbines, ocean currents still offer enormous energy since the density of seawater is over 800 times larger than the air. This makes the industry of ocean current turbines promising and recognizable.

Currently, many countries, leading by Japan and America, are studying and planning on adopting ocean current energy, however, there is still a long way for the development of ocean

current energy. The technology of ocean current turbines starts later than the development of wind energy, even the tidal energy, and there is still much to learn about the nature of ocean currents to make the technology mature. Compared with big scale commercial wind turbines operating all over the world, the commercialization of ocean current turbine is still in the stage of planning. Moreover, the prototypes of ocean current turbines are much fewer compared with wind turbines.

In comparison to tidal turbines which are mainly installed nearshore, the technology of ocean current turbines is behindhand. The industry of tidal turbines has witnessed the development of increasing tidal current concepts and investigation of horizontal and vertical prototype turbines, and planning to reach commercialization recently. Some turbines installed in freshwater rivers to make use of steady water flow are also being developed. These also show a bright future for the ocean current turbine, although it is still developing in the early stage.

One of the substantial developments of ocean current turbines is by the Florida Atlantic University. In 2014, the US Department of Interior’s Bureau of Ocean Energy Management granted permission to install the world’s first ocean current energy test site in the outer continental shelf.

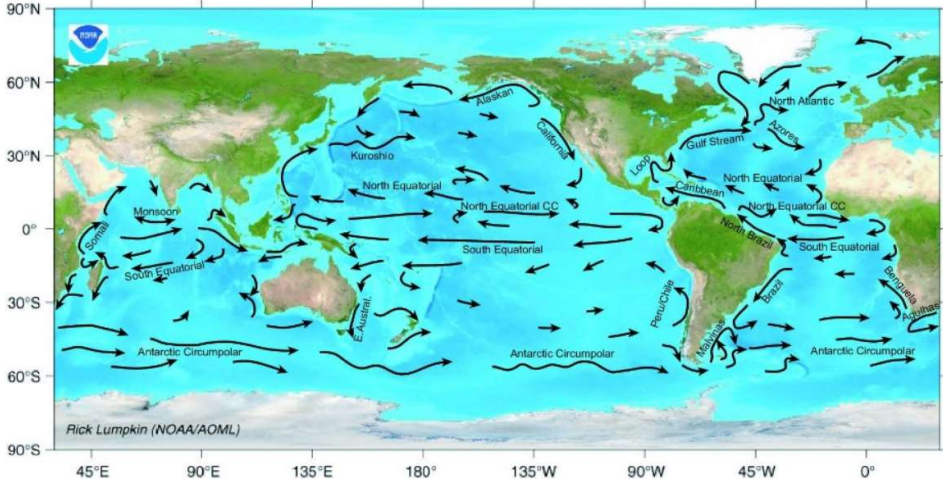


Fig.1.2 Major ocean surface currents [33]

1.1.4 State of the Art in Japan

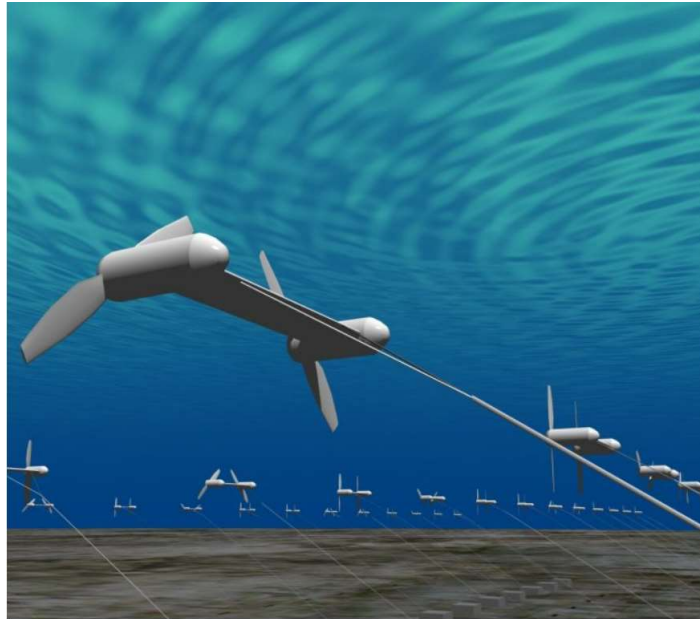


Fig 1.3 Concepts of ocean current turbines in Japan

Floating ocean current turbine project has been studied and developed by the University of Tokyo in cooperation with NEDO and IHI Corporation. The concepts of the ocean current turbines are presented in Fig 1.3. It is expected that this research work will help to develop the industry of ocean energy generation, which will make a contribution to the higher energy security of Japanese society.

Kuroshio Current, as a typical ocean current, offers Japan a good opportunity to adopt the natural renewable energy with little fluctuation in time through time or season. The future industry of ocean current energy will provide a large-scale, constant power source.

In August 2017, NEDO and IHI corporation in Japan completed the verification test of the world's first floating ocean current power generation system as the world's first ocean current power generation of 100 kW off the coast of Kagoshima prefecture, Kagoshima prefecture, as can be seen in Fig. 1.4 [34].

Demonstration tests of the ocean current turbine prototype were conducted by installing a prototype in the Kuroshio Current near the Tokara Islands, yielding a maximum of about 30 kW of power generation output. In the towing test conducted prior to the demonstration test, they achieved the output of the rated output of 100 kW.

Usage of the strong and less fluctuating ocean current energy as a new renewable energy source is expected by NEDO, while IHI aims to commercialize the floating ocean current power generation system in the future.



Fig 1.4 Verification test of the ocean current turbine off Kuchinoshima [34]

1.2 Characteristics of Ocean Current Turbines

1.2.1 Difference between Ocean Current Turbines and Other Turbines

Since the ocean current turbine is considered as a derived technology from the tidal turbine and the tidal turbine technology is more mature than the ocean current turbine, the difference between the tidal turbine is firstly discussed.

Tidal power extracts the energy in the moving tide and converts it into electricity, similar to the way how wind turbines convert wind energy into electricity, but there are some differences.

The energy fluctuation is identified as the principal difference between wind energy and tidal energy. While extreme weather can greatly affect the operation of wind turbines, tides are as reliable as the sunrise and sunset. Among the widely used renewable energy, like wind energy, tidal energy, and solar energy, tidal energy is most predictable. Hence a reliable number of tidal output power can be predicted confidently in tidal energy. This ability to forecast accurately is of critical importance to integrate renewable energy into the electrical grid successfully [35]. The underwater placement of marine turbines offers several advantages, for example, low visual exposure, no noise disturbance to the public and little onshore space occupancy, but also includes several challenges, such as the necessity for waterproofing and salt-proofing techniques, as well as difficult and expensive maintenance.

In the view of design, much of the technology that has been used and developed for tidal current turbines is from wind turbine application. The total kinetic power (P) in a wind turbine or a marine turbine can be calculated by

$$P = \frac{1}{2} \rho A C_p V^3 \quad (1.1)$$

where ρ is the fluid density (kg/m^3), A is the swept area of the turbine (m^2) and V is the fluid velocity (m/s).

C_P is an important parameter in turbine designing, named as power coefficient and is calculated as the percentage of power that can be extracted from the fluid. Betz's law is taken into account for the power loss. The upper limit of the Betz's law, or named Betz's limit, 59.3%, is for the turbine with high efficiency and low mechanical losses. For marine turbines, including tidal turbines and ocean current turbines, C_P is estimated to be between 0.35 and 0.5 [36]. Recently there is no essential difference in C_P between tidal turbines and wind turbines.

It is promising for the industry of tidal turbines about the power output and the turbine scales when compared to the commercial large-scale wind turbines and wind farms in operation. For illustration, Fig 1.5 shows a 1MW tidal turbine against an offshore 1MW wind turbine. Moreover, with stable and highly predictable tidal currents as input, tidal turbines are competitive with the large-scale wind turbines in size and in power output of energy extraction [16, 37].

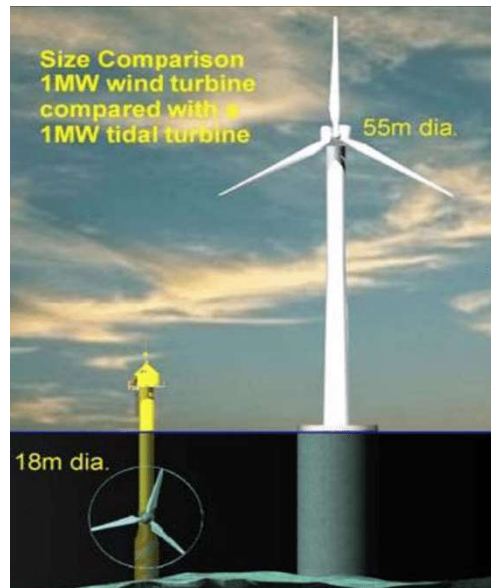


Fig 1.5 A 1MW tidal turbine against a 1MW wind turbine [38]

When it comes to the ocean current turbine, the ocean current velocity is usually lower than the tidal speed, which means that for the same power output, the rotor diameters of ocean current turbines will be bigger than tidal turbines. For the 1MW ocean current turbine prototype model developed by the University of Tokyo, NEDO and IHI, the diameter will be 40 m with

rated current speed of 1.5 m/s, while most of the 1MW tidal current turbines have diameters within 20 m, which can be seen in Table 1.1.

Compared with the tide turbines which are usually installed nearshore, ocean currents have stable energy and the flow is generally in one direction. Although ocean currents have several challenges, for example, variations by seasons, it is irresistible to harness the continuous, significant current energy.

1.2.2 Shear Flow in Ocean Current



Fig 1.6 The Kuroshio Current path [39]

In Japan, Kuroshio Current, shown in Fig 1.6, is recognized as one of the strongest currents in the world. It provides the potential for large-scale ocean current turbines. To make use of this ocean current energy, acoustic Doppler current profiler (ADCP) was used to observe the current flow velocity near Miyake Island for more than one year [40, 41]. When analyzing the observed field data, nearly linear shear flow profile in velocity was discovered with the center of the Kuroshio Current close to the observation location [42, 43]. For one hour averaged data, it shows in Fig 1.7, and three months averaged data are shown in Fig 1.8.

It is noted that these shear flows are observed near sea surface or mid-depth, while the shear flow in the tidal or wind turbine technology means a shear in the boundary layer at the seafloor or land surface.

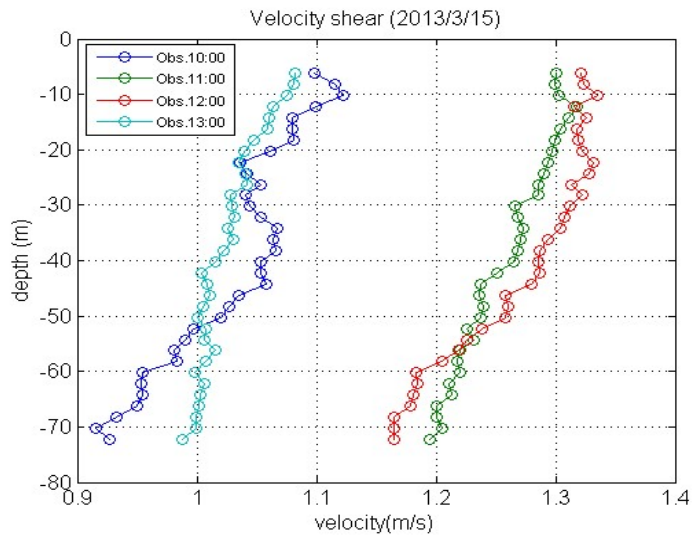
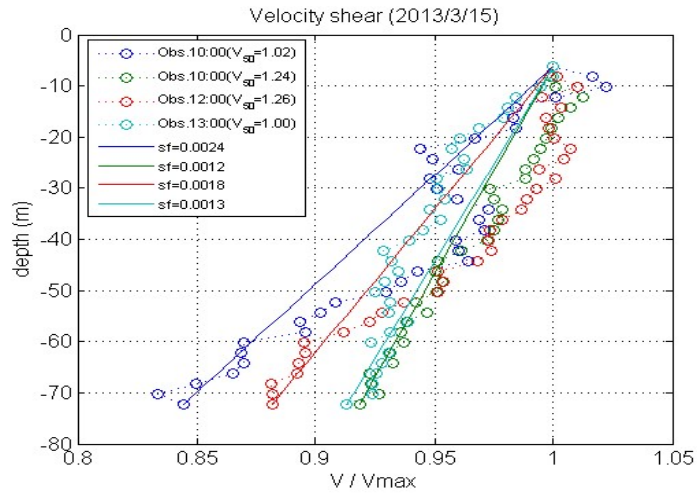


Fig 1.7 One hour averaged current speed in March 13, 2013[42]

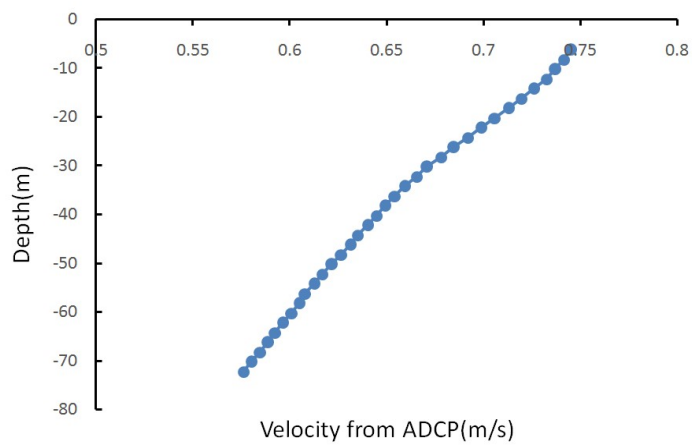


Fig 1.8 Averaged current speed for the period: March 13, 2013 – June 30, 2013[43]

The effect of shear flow is essential for two primary reasons. First, it can cause fatigue of the turbine blades which could result in eventual failure. Second, it causes variations in the output power which gives rise to instabilities in energy yields. Predicting the hydrodynamic characteristics in shear flow is important for using ocean current turbines in this area. In addition, it induces device motions which spoil the integrity of the mooring system. Therefore, it is necessary to find effective methods to investigate proper methodologies for estimating hydrodynamic loads on ocean current turbines and to evaluate the performance in operation of ocean current turbine [17].

1.3 Challenges in Ocean Current Turbines

Floating ocean current turbines can be used to extract energy from the ocean current resources. Although they are similar in function to tidal turbines and floating offshore wind turbines. However, there are still several challenges in establishing effective methods for ocean current turbines designing.

1.3.1 Thrust

Since water is much denser as a medium than the air, the ocean current turbine will experience a high thrust compared with the wind turbine. The maximum thrust of the turbine (T_{max}) can be calculated with the equation:

$$T_{max} = \frac{1}{2} \rho A V_{max}^2 C_T \quad (1.2)$$

where C_T is the thrust coefficient, and V_{max} is the maximum flow velocity (m/s), A is the swept area of the turbine (m²).

With the equation (1.2), it can be calculated that the thrust on a 1MW marine current turbine with a swept area of 1256 m² in a flow of 1.5 m/s is close to 1400 kN. A wind turbine with the same output power 1MW, with a swept area of about 2000 m², in 15 m/s wind experiences about 60 kN thrust. The difference is significant. That is why many tidal turbines use thick blades for structural strength. For ocean current turbines, thick blades are also expected because of high thrust.

1.3.2 Aspect Ratio

Tidal turbines present some distinct features when compared with wind turbines, such as the blade with reduced diameters, as shown in Fig 1.5. For ocean current turbines, the blade diameters have no much difference with wind turbines, because the ocean current speed is expected to be lower than the tidal flow speed.

The aspect ratio A_r is defined as [44]:

$$A_r = \frac{R}{c_{0.75}} \quad (1.3)$$

where R is the radius of the turbine rotor (m), and $c_{0.75}$ is the chord length at 75 percent radius (m).

Since the high thickness of blades caused by high thrust generally leads to long chord, the aspect ratio of ocean current turbines is much smaller than the case of wind turbines.

Ref. [45] discussed that the aspect ratio affects the airfoil performance. For the ocean current turbine design, we need to investigate whether the simulation models for high aspect ratio wind turbines can be applicable to low aspect ratio ocean current turbines.

1.3.3 Solidity

Solidity is recognized as one of the most important parameters having great effect on the horizontal axis turbine performance [46]. For example, changing solidity by changing the blade numbers, may cause great change in power curves, as shown in Fig 1.9. Generally, the small number of blades gives better power coefficient, while it gets bigger torque, thrust and forces.

Definition of solidity is the ratio of the circumference of the turbine rotor containing materials rather than the medium.

Mathematically it is defined as follows,

$$\sigma = \frac{BCR}{A} \quad (1.4)$$

Where B is the blade number, c is the blade chord (m), R is the blade length (m), A is the turbine swept area (m²).

For one turbine blade, solidity varies in different positions on the blade, when near the hub and the blade chord is big, solidity gets the maximum value. On the contrary, solidity is smallest in the blade tip.

It is apparent that for different turbines, the value of solidity is affected by changing the rotor radius to blade chord ratio and blade numbers. Many tidal turbines increase blade numbers to strengthen structure in consideration of high thrust, using four blades or even more. However, in that case, the friction will increase with the drag force.

In our design of ocean current turbines, two blades turbines are adopted for several reasons. First, ocean current turbines with two blades can avoid drag when towed to the designed location, comparing with the turbine of three blades or more. Second, two blades are much easier to transport and install, especially for large-scale ocean current turbine farms. Third, the

power coefficient of two blades is higher than the case of three blades or more, which can offset the decreased number of blades in some degree.

In general, most large-scale wind turbines in operation are three bladed. That means, the performance of our designed ocean current turbines will be different from general wind turbines, which will need attention in the design process.

A performance curve, or named power curve, is used for rating turbine performance, expressing the power coefficient (C_p) as a function of tip speed ratio (TSR). No turbines are supposed to exceed the limit value of 0.593 for power coefficients. That limitation is called the Betz limit. For different types of turbines, the expected power curves are shown in Fig 1.9, showing that 2-bladed model has higher power coefficient than models with three blades or four blades.

On the other hand, as discussed above, ocean current turbines have higher thickness and chord values compared with wind turbines, which will also affect the solidity.

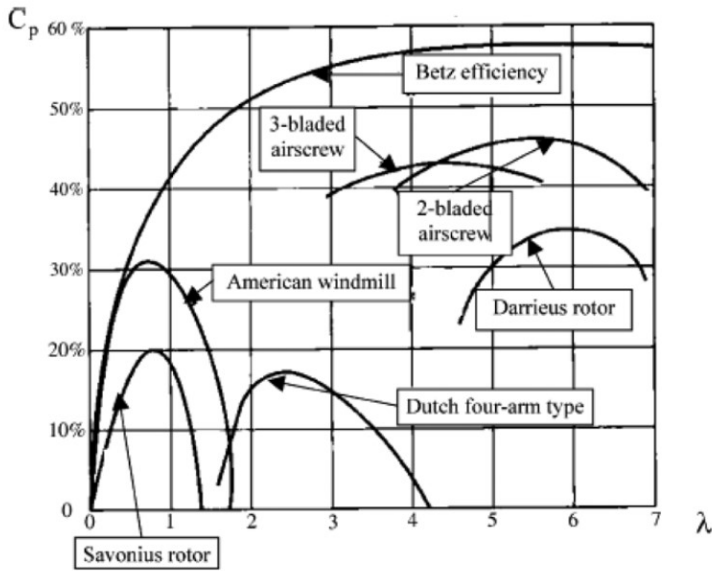


Fig 1.9 Expected performances of different types of turbines [47]

In addition, when calculating BEM model of ocean current turbines with tip loss correction and hub loss correction, the loss factors are also affected by the solidity. Compared with wind turbines, the accuracy of these corrections on ocean current turbines may be affected by the change of solidity.

1.4 Literature Review

1.4.1 Previous Research Works

The Blade Element Momentum (BEM) method for blade aerodynamic load calculation is considered as the simplest method and is still widely used in wind turbine blade engineering applications [48, 49, 50]. Using this method, it is possible to perform aerodynamic design of a blade rotor and evaluates the performance of turbines with different design conditions [51]. Through the implementation of the model, the rotor can be designed to optimize the geometry of the turbine, such as blade airfoil, turbine diameter, blade chord, as well as to predict and evaluate the thrust, torque of each rotor element and power. Turbine performance in different wind speeds can also be evaluated. Based on the theory by Glauert [51], The BEM theory is modified for application to wind turbines. Recently researchers have made some modification and correction on the BEM theory to improve its accuracy, such as Spera [52], Buhl Jr [53], and Shen et al. [54].

GH Bladed is a famous commercial software based on BEM theory for wind turbine design. Recently, that company has developed GH-Tidal Bladed for tidal turbine design. SERG-Tidal is mainly based on the BEM theory. The results from both codes compared with experiments data show good agreement in the performance of ocean current turbine, including the power output and thrust, in uniform flow. However, the power coefficients GH-Tidal Bladed code predicts are higher than experiments, while the thrust coefficient estimated by SERG-Tidal is lower. This study proves that the BEM model can be an effective developing tool for the design of marine current turbines.

To harness the tidal energy effectively, it is of great importance to find the proper sites with high tidal flow speeds and high power yields for tidal turbines. Therefore, the characteristics of tidal flow speed and turbulence become major terms to learn before design. Up to date, generally, studies of wind farms contribute to how to deploy tidal turbines [15, 18], but more

studies on simulation and experiments of tidal turbines have been done in recent years. Myers et al. [36,37] conducted experiments on a 0.4 m diameter turbine and measured the wake with the investigation of its impact. Sun et al. [55] presented the effect of the free surface on the wake of tidal turbines using different flow models. Batten et al. [56] simulated the wake by 2D CFD, focusing on the study of turbulence effect of the upstream turbines on the downstream turbines. It was found that turbulence intensity can be greatly altered for the downstream turbines. There are some further experimental studies on the performance assessment of tidal turbines [57].

It is also necessary to evaluate turbine hydrodynamic performances. There exist several commercial and academic codes based on BEM theory [17, 58], including commercial software named 'Tidal Bladed' which is developed by the world's leading classification society DNV-GL [59]. These methods are mainly from the principals of wind turbines. Examples of the BEM approach include the work of McCann [60], who used GH Tidal Bladed to model the effects of turbulence intensity in the free stream and the wave height on the out of plane forces on turbine blades.

Experimental verifications of two numerical predictions codes are conducted in Ref. [17, 37] for the performance evaluation of tidal current turbines. For a 0.8 m diameter turbine model, experimental measurements were conducted in a cavitation tunnel and a towing tank. Two simulation tools were introduced and verified, including commercial code (GH-Tidal Bladed) and an academic code (SERG-Tidal).

CFD models offer insight into the flow field around the device in 2 or 3 dimensions and are capable of predicting the interaction of the flow with devices. Some CFD studies of wind and tidal turbines use the simplified "actuator disc" models of the turbine blades where the turbine is modeled as a porous disc through which the flow passes. Sun et al. offered an example case of this method [61].

Ref. [62] (2007) conducted a wake study of a horizontal axis tidal current turbine that was scaled to 1/30. In the experimental circulating water channel, they tested the model turbine with 0.4 m diameter, measured turbine performance parameters and turbine thrust over a range of tidal current velocities. Their experimental results show that early investigations are important before installing arrayed tidal current turbines to avoid the effects of blockage [62]. Ref. [63] (2007) measured the power and thrust of tidal current turbines in different pitch angles and flow speeds in a cavitation tunnel. The test was carried out on a tidal current turbine with a diameter of 0.8 m, a 2.4 m x 1.2 m tunnel cavitation and a 60 m long towing tank. The results presented a single turbine operation and performance changes with different rotor tip immersion. The results show that the solid wall cavitation tunnel can be used for the test of tidal current turbine models. Ref. [64] (2008) described a diffuser-enhanced floating tidal current turbine. They researched on how to optimize device geometry for higher power extraction. They also presented the use of large rotors to extract power from channel water flows. Ref. [65] (2012) presented on flow distribution and generation for ducted composite ocean current turbines using CFD. They introduced a way to produce a ducted composite tidal current turbine with high performance over conventional geometry. The lightweight ducted composite tidal current turbines can be fast and economical.

Ref [66] (2009) described the effects of ocean current turbine on the marine environment of America with the adoption of open turbines to generate electricity in the Florida ocean. These open flow turbines provide a harmless pathway for marine species. However, the maintenance and turbine installation can damage marine life and the marine environment. Ref [67] (2010) conducted a study based on numerical techniques to study the optimal turbine layout in seawater. From the flow of these turbines, they found the best turbine layout that would yield the maximum power. According to the study, the distance between two turbines was recommended to be approximately three times the diameter of the ocean current turbine.

They suggested the arrangement of such an ocean current turbine to maximize the use of current energy to generate electricity. Ref [68] (2013) tested on an optimized ducted tidal current turbine. The ducted rotor is free to rotate around a vertical axis fixed to the floor. They used a numerical model based on Navier-Stokes calculation to analyze the flow in the duct. They also obtained flow calculations in the pipeline through experiments. In addition, the economic price of the pipeline is evaluated as the key parameter for finalizing the project's feasibility. Their future plan is to study the turbine stability, how to change with the current direction, and the superposition with waves for ocean current turbines.

1.4.2 Numerical Study on Turbine Unsteady Loads

In the study of ocean current turbine loads, a cyclic variation in attack angle in the blade section is major unsteadiness, which will be discussed later. Thus, based on this condition, we aim to find a better methodology than classical BEM theory. It is mentioned that most of the knowledge on the unsteady load on the blade comes from the wind turbine industry. Several important mathematical models based on the variety of inflow conditions and relevant works are reviewed here.

1.4.2.1 Dynamic Inflow Model

Carpenter et al. [69] developed the dynamic inflow model to consider unsteady aerodynamic lag of the inflow over the turbine in response of blade pitch and turbine thrust. The mathematical model includes the concept of the BEM theory. The ordinary differential equations are used to present an aerodynamic model.

The method showed advantages for structural dynamic and aeroelastic analysis of the helicopter rotor, because the coupled problem can be solved using the same numerical method. Pitt et al. [70,71,72,73] further developed it for helicopter applications. Hansen [74], Bierbooms [75], and Snel et al. [76] discussed dynamic inflow models to apply it to wind turbine field.

1.4.2.2 Vortex Wake Model

The vortex wake model assumes for incompressible potential flow and solves the induced velocity applying the Biot-Savart law. Although the vortex wake model requires less computational time than the CFD, it still has a disadvantage of computational efficiency, because of the necessity to calculate the Biot-Savart law many times.

Clark and Leiper [77] developed the free vortex wake model to apply it for the helicopter rotor. This model has become a widely used tool in the helicopter industry. However, there is

still not yet to see a significant application for the wind turbine study because of the low computational efficiency.

1.4.2.3 Unsteady Model on Blade Section

When considering the unsteady aerodynamics of the wind turbine blade sections, two-dimensional models are common for blade element calculation. There are several mathematical models to simulate unsteady airfoil effects.

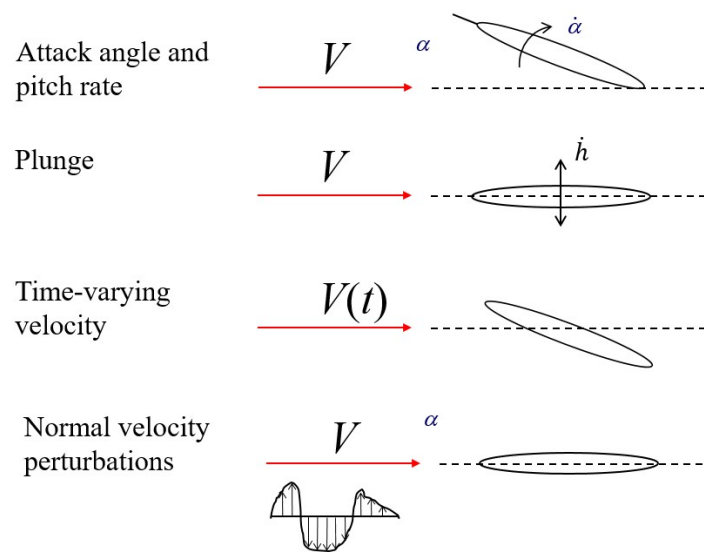


Fig 1.10 Decomposition of forcing into perturbations to local attack angle and velocity field [78]

For the blade element, Fig 1.10 shows the decomposition of forcing into perturbations to the local attack angle and velocity field. The unsteady effects from various types of forcing should be treated in different ways, and it is necessary to consider the aerodynamic response to each component of forcing separately.

The incompressible, unsteady airfoil theory has been developed both in the frequency domain and in the time domain, by Wagner [79], Theodorsen [80], Küssner's [81], and von Kármán & Sears [82]. Bisplinghoff et al. [83] discussed all the models and Leishman [94] offered further details about the application.

Theodorsen's function [80] is recognized as a useful tool in the unsteady thin-airfoil theory, which represents the effect of periodic variations in the angle of attack. In Theodorsen's theory, the lift can be expressed as a function of the reduced frequency, which is an important parameter for the unsteady theories. Theodorsen's theory is suitable for our problem, because the periodic variation of the attack angle is a major issue in our problem.

Theodorsen lift can be divided into circulatory part and non-circulatory part. Adding the non-circulatory part leads to decrease of the total lift amplitude. The lift amplitude increases with the reduced frequency, and the phase angle changes at high reduced frequency, where the non-circulatory part is dominant. Theodorsen's unsteady theory has advantages of simplicity both in mathematics and computation. Leishman [84] shows the agreement between measurement and the simulation using Theodorsen's function of the unsteady lift on airfoils oscillating in plunge and pitch oscillations.

For applying to the turbine rotor disk, von Kármán & Sears [82] solved a problem of nonuniform induced velocity. The theory dealt with a problem of a thin airfoil moving through a sinusoidal vertical velocity field. Similar to Theodorsen's solution, it is also in the frequency domain. Sears [85] discussed how to apply the theory to other conditions such as steady oscillations and a sharp-edge gust.

Wagner [79] solved the thin-airfoil problem in time domain with a step change of attack angle. There are several similarities with Theodorsen's function, for example, assumption of straight and semi-infinite wake, with strength varying in the chordwise direction according to Kutta condition. Garrick [86] investigates the correlation of Wagner's function and Theodorsen's function.

Küssner [81] studied the response on an airfoil entering a sharp change in vertical upwash velocity. There is a slight difference between Küssner's problem and Wagner's problem. In

Küssner's problem the quasi-steady attack angle changes progressively as the airfoil goes into the change in vertical velocity, while in Wagner's problem, the attack angle changes instantaneously over the whole chord.

Loewy [87] also studied the problem of helicopter rotors. In Loewy's model, the shape of the wake is helix and, in a blade section, the wake is assumed to be represented by layers of vortex, which are decided by the velocity of inflow, blade numbers and rotational period of the rotor. Other assumptions of Loewy's theory are the same as assumptions of Theodorsen's theory. Thus, it can be used to investigate the effect of helical trailing vortex.

1.4.3 Experimental Investigations on Unsteady Loads

In the experimental studies on the tidal turbine, there are various studies on the unsteady loads. Maganga et al. [88] obtained the average thrust on a 3-bladed tidal turbine with a 0.70 m diameter mounted on a tower structure, which is about 1/30 scale, with TI (turbulence intensity) in the flow varying from 8% to 25%. Nevertheless, this experiment didn't report the turbulence spectral characteristics and thrust fluctuations. The effect of turbulence intensity is difficult to be estimated.

There are some experiments on wave effects. Barltrop et al. [89] reported an experiment to measure the thrust for a tidal turbine testing in a towing tank with surface waves. For surface waves with small amplitude and low frequency, Galloway et al. [90] reported no acceleration effect when the bending moment response is compared with the BEM model. However, it is difficult to determine the contribution of the circulatory and non-circulatory term. In addition, it is particularly challenging to infer the load phase lag with small value in the measurement of the free surface.

Milne [91] and Milne et al. [92] used a sub-carriage on the towing carriage to make variation of inflow velocity with a 0.37m radius three-bladed rotor, and measured the thrust and the out of plane bending moment. This study shows significant unsteady load when the turbine is at optimal power output. However, this large effect may be influenced by the boundary layer separation and the dynamic stall on the blade. It also shows the effect of high tip speed ratios. For the cases of high tip speed ratios (tip speed ratios more than 5), it generally comes along with the absence of dynamic stall, and the response tends to be relatively more linear. Thus proper experiments with similar high tip speed ratios were considered as a good choice to quantify the circulatory part and the non-circulatory part.

There is no significant research on experiments of tidal turbines or ocean current turbines in unsteady shear flow, there is thus need to conduct experiments to generate shear flow and test the ocean current turbine model in the shear flow.

1.5 Purpose of the Study

In the field of wind turbines, many convenient technical tools based on the classical BEM are used as standards. These tools are utilized for the design of tidal turbines, and they may be applicable to the ocean current turbines. However, as discussed in the previous sections, several differences exist between the ocean current turbines and the wind turbines, such as the high thrust, the solidity, the aspect ratio and so on. Information on marine propellers [93] may give guidance to the investigation of ocean current turbines. However, the shape of marine propellers is totally different from the ocean current turbine. Thus, it is necessary to understand whether the methods widely used for wind turbines are effective for ocean current turbines.

In the case of ocean current turbines, a shear flow observed near the ocean surface is one of the important issues, because it induces a periodic fluctuation of the attack angle in a blade section. As a result, a cyclic load on the turbine blade is induced, which causes a fatigue damage. In case of a floating ocean current turbine, fluctuation of the inflow induces motions of floating body and the motions create a cyclic fluctuation in the relative inflow velocity to the turbine. Thus, it is important to predict accurate forces and moments on the blade. Although it is out of scope of the thesis, it is also important to apply the estimated load to the simulation of the body motion, which is used for a time-consuming prediction of long-term statistics or evaluation of a turbine control system. Therefore, the estimation method should be simple and not time-consuming.

Although both CFD and vortex wake model may offer high accuracy in the load estimate, they are not the best choice for the motion simulator, because of the required large computational resource. For this reason, the combination of the classical BEM based method and the two dimensional unsteady theory is used in this study. Since the periodic fluctuation of the attack angle is important as aforementioned, Theodorsen's theory is used. The shortcoming is the simplification of the effect of trailing vortex, since Theodorsen's theory assumes a single straight trailing vortex. Therefore, the results will be compared with Loewy's theory. The

estimated results are also compared with experimental results for validation. These are discussed in Chapters 3 and 4.

In summary, the purpose of the study is to develop a simple and accurate model for blade load simulation of ocean current turbines in shear flow based on the classical BEM and Theordosen's theory, so that the model can be easily coupled with the calculation of motion and other turbine behaviors. Moreover, to validate the numerical model, a shear flow generating system is established in the circulating water channel and measurements of the out of plane bending moments at the blade root is performed.

It is noted that the out of plane bending moment at the blade root is the most important load for the blade design. Therefore, the out of plane bending moment at the blade root (M_y) is the focus in this study. For wind turbines, M_y is suggested as an important design load in 50-year storm and extreme operational conditions by international guideline [94].

1.6 Thesis Outline

This thesis is organized as follows:

Chapter 1 describes the motivation of the thesis, and the newest information on the development of marine current turbines and ocean current turbines. Also, the challenges in ocean current turbine are introduced and the problem of unsteady loads of ocean current turbines in shear flow are brought up.

Chapter 2 introduces the classical BEM theory and all the corrections for simulation of current turbine loads as a theoretical background. This theory is then utilized to simulate the performance of the blades and compared with experimental results of other scholars.

Chapter 3 deals with experiments conducted to generate shear flow in the circulating water channel and the experimental results are compared with the results by the classical BEM.

Chapter 4 proposes how the Theodorsen's function is combined with the classical BEM theory to consider the unsteady effect. It leads to increased accuracy for the simulation results with experimental validation.

Chapter 5 discusses in detail on several parameters effecting the simulation and advice on design of ocean current turbines.

Chapter 6 makes the conclusions of the thesis.

2 . BEM Theory for Ocean Current Turbine

2.1 BEM Theory

In the turbine industry, classical BEM theory is widely used as a computational tool to predict the blade loads and rotor power performance. It is a combination of two theories, the momentum theory, and the blade element theory. The momentum theory describes a momentum balance on a rotating annular stream tube passing through a turbine. Dividing the rotor blade into several blade element sections, the blade element theory can be used for the section lift and drag forces calculation.

2.1.1 Momentum Theory

To analyze the hydrodynamic behavior of the ocean current turbine rotor, the mechanics of rotor power absorption from ocean current resources are first considered in the energy extraction process. In the momentum theory, the rotor of the ocean current turbine is replaced by an “actuator disk” through which witnesses discontinuous decrease in the static pressure, as depicted in Fig 2.1.

The assumptions of the momentum theory are as follows:

- 1) Ocean current turbine rotor is modeled as an actuator disk, adding momentum and energy to the flow
- 2) Steady, inviscid, irrotational, incompressible flow.
- 3) Flow is uniform through the rotor disk and in the far wake.
- 4) No wake swirl.

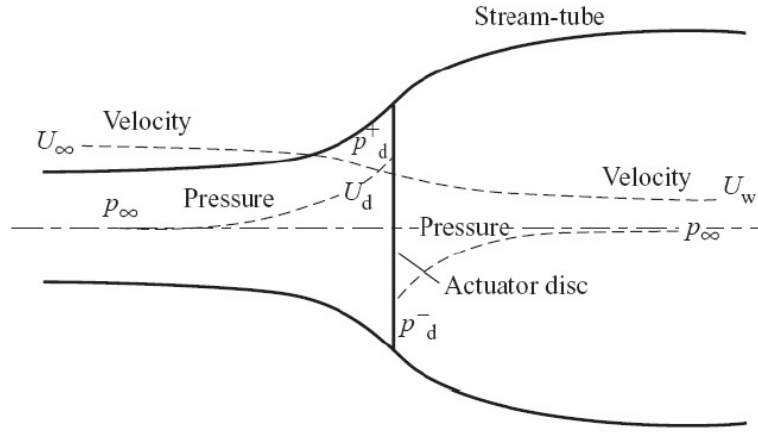


Fig 2.1 Actuator disc and stream tube concept [94].

Since the flow is incompressible along the stream tube, the mass flow is the same everywhere. Per unit time, the mass conservation yields,

$$\rho A_{s\infty} U_{\infty} = \rho A_{sd} U_d = \rho A_{sw} U_w \quad (2.1)$$

where ρ is the fluid density (kg/m^3), A_s is the section area (m^2) and U is the flow velocity (m/s). The symbol ∞ refers to conditions far upstream, d refers to conditions at the disk and w refers to conditions in the far wake. The velocity difference induced by actuator disc must be superimposed on the free stream velocity as induced velocity. This induced velocity is expressed by aU_{∞} , and a is named the axial induction factor. Then the velocity at the disc can be expressed as,

$$U_d = U_{\infty}(1 - a) \quad (2.2)$$

Although the engineering principles of horizontal ocean current turbines are close to wind turbines, we still need to consider the effects of different thrust, aspect ratio, solidity, and most importantly, shear flow profile.

2.1.2 Induction Factor Calculation

The classical BEM theory combines the momentum theory with the blade element theory. From the momentum theory originally by Ref. [51], the annular thrust dT_I and annular torque dQ_I can be calculated as,

$$dT_1 = 4a(1 - a)\rho U_\infty^2 \pi r dr \quad (2.3)$$

$$dQ_1 = 4\pi\rho a' \Omega U_\infty (1 - a) r^3 dr \quad (2.4)$$

where a is the axial induction factor, similarly, a' is the tangential induction factor, r is the local blade radius (m), dT_I is element thrust (N), the dQ_I is the element torque (N*m), ω is the angular velocity of the wake (rad/s) and Ω is the angular velocity of the ocean current turbine (rad/s).

In the blade element theory, the ocean current turbine blade is divided into several separate 2D airfoil element section. It is assumed that each section has no interaction with each other. The flow at each blade element has associated axial velocity and tangential velocity, with the inflow angle (θ). The lift and drag forces on the blade sections of ocean current turbines can be obtained by airfoil equations :

$$dL = \frac{1}{2} C_L \rho W^2 c dr \quad (2.5)$$

$$dD = \frac{1}{2} C_D \rho W^2 c dr \quad (2.6)$$

where c is the blade chord (m), W is the relative fluid velocity (m/s). Lift coefficients (C_L) and drag coefficients (C_D) can be obtained as a function of attack angle (α) in certain Reynold number. From the geometrical twisting angle (β), the inflow angle (θ) and pitch angle of the rotor (θ_p), the attack angle can be calculated by,

$$\alpha = \theta - \beta - \theta_p \quad (2.7)$$

$$\tan\theta = \frac{U_\infty(1-a)}{\Omega r(1+a')} \quad (2.8)$$

In classical BEM theory there is an assumption that only the forces on the corresponding blade sections cause the change in momentum of each annular section, since different elements have no interaction with each other. The axial and tangential force equations from each theory are expressed as follows, where c is the blade chord (m), B is the number of blades, dT_2 is element thrust (N), the dQ_2 is the element torque (N*m):

$$dT_2 = \frac{1}{2} \rho W^2 B c (C_L \cos\theta + C_D \sin\theta) dr \quad (2.9)$$

$$dQ_2 = \frac{1}{2} \rho W^2 B c (C_L \sin\theta - C_D \cos\theta) r dr \quad (2.10)$$

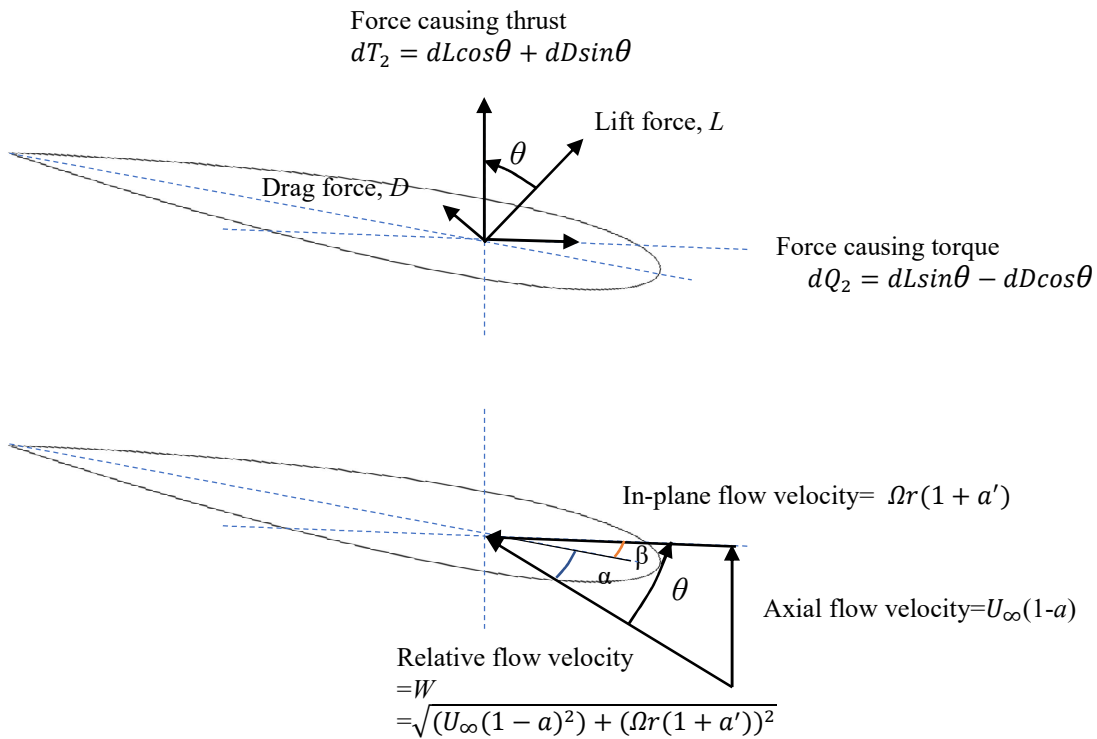


Fig 2.2 Forces and velocities on a blade section

where σ_r is the local blade solidity, which can be expressed by $Bc/2\pi r$. Axial and tangential induction factors can be expressed as follows:

$$\frac{a}{1-a} = \frac{\sigma_r(C_L \cos\theta + C_D \sin\theta)}{4\sin^2\theta} \quad (2.11)$$

$$a = \frac{1}{\frac{4\sin^2\theta}{\sigma_r(C_L \cos\theta + C_D \sin\theta)} + 1} \quad (2.12)$$

$$\frac{a'}{1+a'} = \frac{\sigma_r(C_L \sin\theta - C_D \cos\theta)}{4\sin\theta \cos\theta} \quad (2.13)$$

$$a' = \frac{1}{\frac{4\sin\theta \cos\theta}{\sigma_r(C_L \sin\theta - C_D \cos\theta)} - 1} \quad (2.14)$$

Fig 2.2 shows the lift force (L), drag force (D), also the velocity components of one blade element in BEM theory, where Ω is the angular velocity of rotor (rad/s).

Because the lift coefficients and drag coefficients are non-linear with the attack angle, the induction factors a and a' must be solved iteratively. Finally, a and a' values for each radial station can be obtained by defining an objective function g_L and minimizing g_L to 0 using Newton Raphson function, given by

$$g_L = (dT_1 - dT_2)^2 + (dQ_1 - dQ_2)^2 \quad (2.15)$$

Iterative procedure is as follows:

1. Divide the whole blades into several airfoil sections.
2. Give chord length c , blade twisting angle β , and pitch angle θ_p as a function of local blade radius r for each section.
3. Define inflow speed U_∞ and rotor angular velocity Ω .
4. For a blade section of radius r :

- 1) Give the initial induction factors a and a' . (We used $a = a' = 0$.)
- 2) Calculate the flow angle θ by equation (2.8).
- 3) Calculate the local attack angle α by equation (2.7).
- 4) Obtain lift coefficient C_L and drag coefficient C_D for attack angle α from the airfoil used.
- 5) Calculate dT_1 , dQ_1 and dT_2 , dQ_2 respectively by equation 2.3, 2.4, 2.9 and 2.10.
- 6) Calculate g by equation (2.15).
- 7) If g is more than a certain tolerance (0.00000001), give new values to induction factors according to Newton Raphson function, and return to step 2).
- 8) Calculate the forces and moments on the blades by equation (2.15), (2.16) and (2.17).

Flow chart of induction factor calculation is shown in Fig 2.3.

After obtaining all the section thrust and torque, the thrust and torque of the turbines can be calculated by

$$T = \int_{R_{hub}}^R dT_1 \quad (2.16)$$

$$Q = \int_{R_{hub}}^R dQ_1 \quad (2.17)$$

where R is the radius of turbine rotor (m), R_{hub} is the radius of turbine hub (m), T is the rotor thrust (N) and Q is the rotor torque (N*m).

The out of plane bending moment at the blade root M_y (N*m) is calculated by the following equation:

$$M_y = \int_{R_{hub}}^R r dT_1 \quad (2.18)$$

The tip speed ratio (TSR), power coefficient (C_P), thrust coefficient (C_T), non-dimensional flapwise bending moment coefficient (C_{my}) are defined as follows:

$$TSR = \frac{\Omega R}{U_0} \quad (2.19)$$

$$C_P = \frac{Q\Omega}{0.5\rho AU_0^3} \quad (2.20)$$

$$C_T = \frac{T}{0.5\rho AU_0^2} \quad (2.21)$$

$$C_{my} = \frac{M_y}{0.5\rho ARU_0^2} \quad (2.22)$$

where U_0 is the free stream velocity at turbine hub center (m/s).

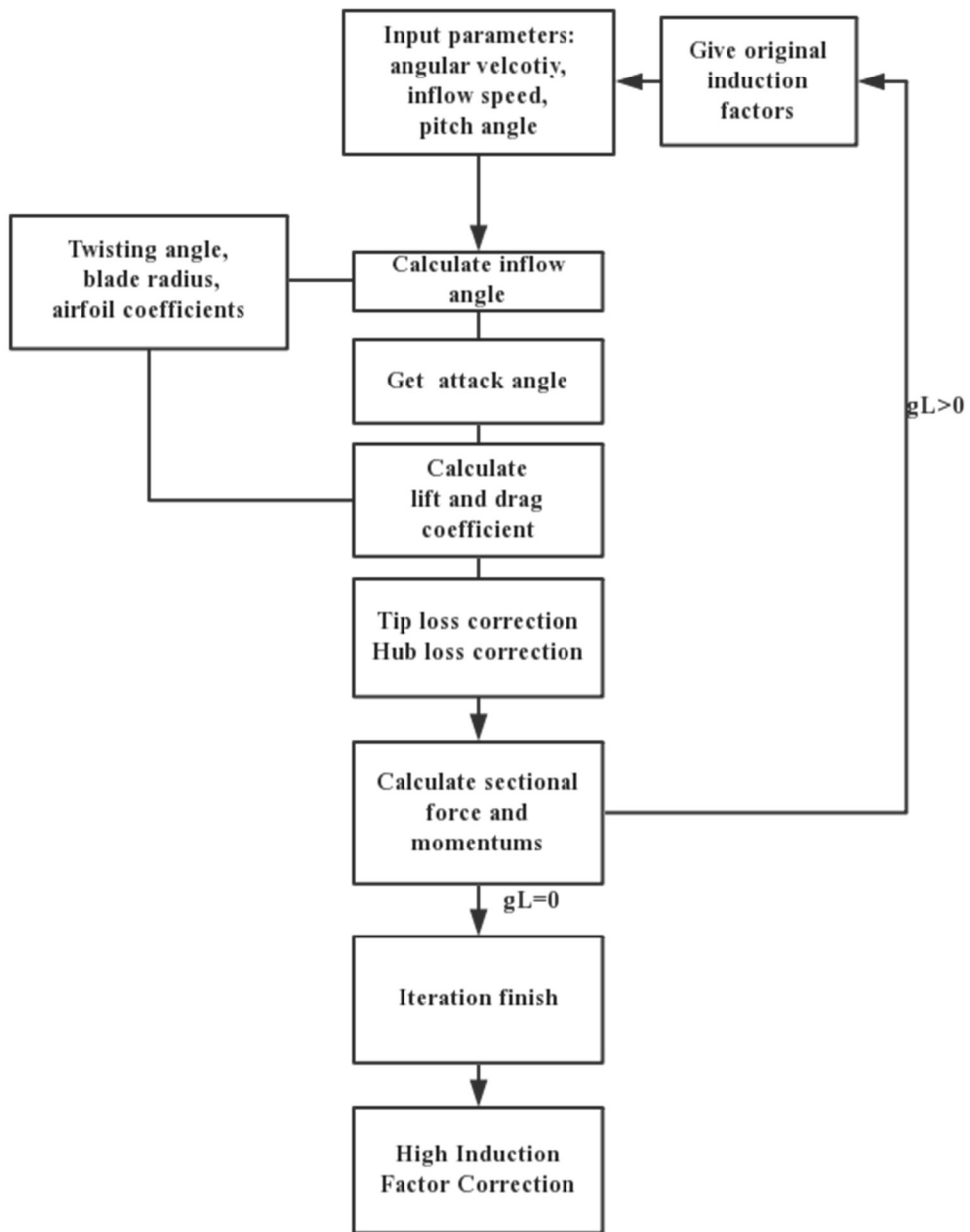


Fig 2.3 Flow chart of induction factor calculation

2.1.3 Limitation of Classical BEM Theory

Limitations of the classical BEM theory can be found in the assumptions. The classical BEM theory assumes steady fluid field around each blade element and instantaneous acceleration in the passing flow to adjust to the changes in the wake [93].

The classical BEM theory doesn't work if the blades suffer large deflections in the out plane of the turbine rotor. However, this doesn't happen in our case with the ocean current turbines.

Blade element theory assumes that the forces acting on the blade element are essentially 2D. Corrections, such as the use of Prandtl's tip loss correction and hub loss correction, should be adopted to consider 3D effects.

Static airfoil characteristics, such as the nonlinear changes in the lift with the stall, can also be incorporated into the classical BEM theory.

In practice, seldom is the case that only the original theory is used for the calculation or design of turbines blades. As for the ocean current turbines, when developing a simple method for the load analysis, several principal corrections should be incorporated with classical BEM theory to improve accuracy. Common applications will be discussed in the following part, such as the tip loss correction and hub loss correction, thrust correction and correction after stall.

2.1.4 Tip Loss Correction

Tip loss correction is widely recognized as one of the most important corrections for original theory. In this correction, the fact that the variation of axial induction factor over the rotor area is considered. Most of the tip loss theory based on Prandtl's model, which is based on simplified vortex theory. Prandtl assumed optimal operating condition and no wake expansion in his theory, as discussed in Ref. [95]. Span-wise flow with finite number blades will produce vortex distribution that results in variation in induction factors local to the blade tip.

Prandtl's model in Ref. [95] expressed the tip loss factor with the reduction estimation in wing elemental force at the blade tips by:

$$F_{tip} = \frac{2}{\pi} \cos^{-1} e^{-f_{tip}} \quad (2.23)$$

where the term f_{tip} can be solved by:

$$f_{tip} = \frac{B}{2} \frac{R-r}{r} \frac{1}{\sin\theta} \quad (2.24)$$

2.1.5 Hub Loss Correction

Hub loss correction is a correction similar to tip loss correction. However, the reduction of wing elemental force is caused by the hub instead of the tip. Hub loss correction estimates the influence of the vortex that is close to the hub of the turbine rotor. Ref. [96] suggests the momentum equations in original theory apply with a hub loss correction model as follows,

$$F_{hub} = \frac{2}{\pi} \cos^{-1} e^{-\frac{B}{2} \frac{r-R_{hub}}{R_{hu}} \frac{1}{\sin}} \quad (2.25)$$

In practical, the hub loss correction is usually combined with tip loss correction as a combined loss correction factor expressed by:

$$F = F_{tip} F_{hub} \quad (2.26)$$

Then using the above overall loss factor as a multiplication factor into the momentum equation, equation (2.3) and (2.4) can be replaced as:

$$dT_1 = 4\pi\rho U_0^2 a(1-a)Frdr \quad (2.27)$$

$$dQ_1 = 4\pi\rho a'\Omega U_0(1-a)Fr^3dr \quad (2.28)$$

Other equations in the classical BEM theory are unchanged.

Finally, induction factors, a and a' values for each element section can be obtained by defining and minimizing g_L , given by iteration of the Newton Raphson function in the equation (2.14).

2.1.6 High Induction Factor Correction

When the axial induction factor a is small, original theory can well predict the thrust. However, as the axial induction factor rising to over certain value, the momentum theory will no longer be reliable. With the increase in the axial induction factor, the flow patterns through the turbine become much more complicated that prediction by momentum theory becomes invalid [97, 98].

High Induction Factor correction developed by Glauert [97], including tip and hub losses, is empirically used as,

$$\begin{aligned} \text{For } a \leq \frac{1}{3}: & \quad dT_1 = 4\pi\rho U_0^2 a(1-a)Frdr \\ \text{For } a > \frac{1}{3}: & \quad dT_1 = 4\pi\rho U_0^2 a\left(1 - \frac{a}{4}(5-3a)\right)Frdr \end{aligned} \quad (2.29)$$

Based on Glauert's correction, Spera [52] made modifications of the high induction factor correction as follows,

$$\begin{aligned} \text{For } a \leq a_c: & \quad dT_1 = 4\pi\rho U_0^2 a(1-a)Frdr \\ \text{For } a > a_c: & \quad dT_1 = 4\pi\rho U_0^2 (a_c^2 + (1-2a_c)a)Frdr \end{aligned} \quad (2.30)$$

where a_c is approximately 0.2, F is Prandtl's tip loss factor with hub loss factor and corrects the assumption of an infinite number.

Equation (2.30) is used in the iteration of the original theory. In Fig 2.4 the two expressions for thrust coefficient C_T with axial induction factor a are plotted for overall correction factor $F = 1$ and compared with the momentum theory.

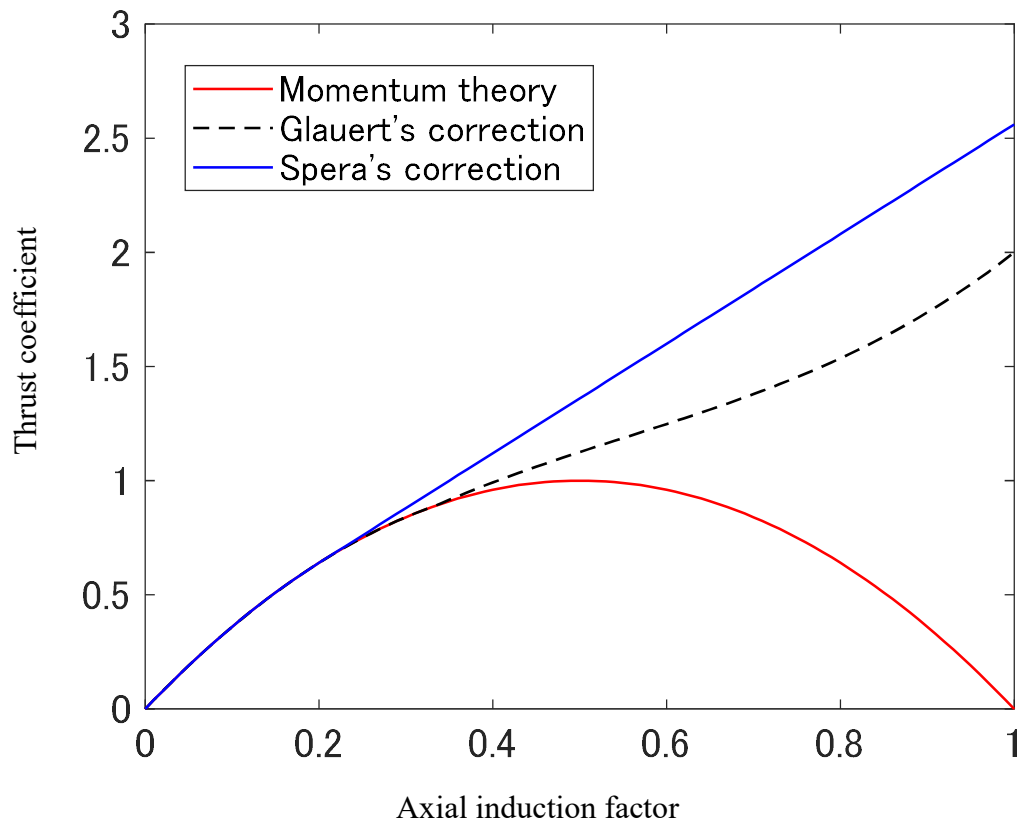


Fig 2.4 Different expressions for the thrust coefficient C_T with the axial induction factor a

After the tip loss, hub loss and high induction factor correction, then the thrust, torque and out of plane bending moment at blade roots can be calculated as Equation (2.16), (2.17) and (2.18). The whole procedures of classical BEM calculations are shown in Fig 2.3.

2.2 Blade Element Coefficients

In this study, NACA0012 airfoil was used for the section shapes of the turbine model. To obtain airfoil data for BEM calculation, using databases such as the database from NREL [99], the databases located at the University of Illinois Urbana-Champaign [100] is possible. However, it is of difficulty to find actual data especially when Reynolds numbers are low for the turbine models.

Bahaj et al. [33, 98, 101] introduced the use of a code to predict 2-D airfoil performance, XFOil [102]. XFOil is a combination of a linear vorticity stream function panel method and a viscous boundary layer solution.

To calculate for the blade elements (airfoil NACA0012), the lift and drag coefficient data are necessary. We also employed XFOil for calculation. For the blade geometry, we used the chord, and twisting angle distributions in Table A.3.

According to Ref. [103], Reynolds number used in XFOil (Re_{XFOil}) is defined by,

$$Re_{\text{XFOil}} = \frac{\rho \sqrt{U_0^2 + (1.4\pi nR)^2}}{\mu} c_{0.7R} \quad (2.31)$$

where $c_{0.7R}$ is the chord length at 70 percent radius (m), n is the turbine rotational rate, U_0 is the free flow speed at the turbine hub center, μ is the dynamic viscosity, ρ is the fluid density.

Thus, we obtained the lift coefficients and drag coefficients for the attack angle ranging from -10° to $+20^\circ$ from XFOil calculation.

In relatively low attack angles, the lift coefficient and drag coefficient agree well with the experimental data from Ref. [104]. Ref. [105] tested NACA airfoils in wind tunnel, though the power coefficient is sensitive with variation of drag coefficient. The results also agreed well

with the pressure distributions and lift coefficients of XFOil results with underestimation of drag coefficients at incidences approaching the stall angle.

For the stall, an alternative method by Viterna and Corriganis [44] is used to calculate the coefficients for high attack angles over the stall angle. The lift coefficients and drag coefficients are computed using following equations:

$$C_L = \frac{C_{D,max}}{2} \sin 2\alpha + A_L \frac{\cos^2 \alpha}{\sin \alpha} \quad (2.32)$$

$$C_D = C_{D,max} \sin^2 \alpha + A_D \cos \alpha \quad (2.33)$$

where A_L and A_D are given as:

$$A_L = (C_{L,s} - C_{D,max} \sin \alpha_s \cos \alpha_s) \frac{\sin \alpha_s}{\cos^2 \alpha_s} \quad (2.34)$$

$$A_D = C_{D,s} - \frac{C_{D,max} \sin^2 \alpha_s}{\cos \alpha_s} \quad (2.35)$$

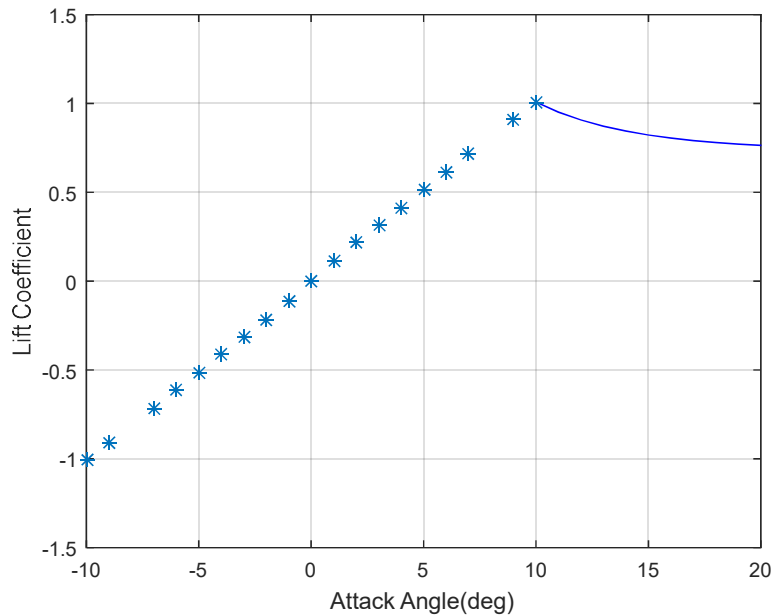


Fig 2.5 2-D lift coefficient data of NACA0012 airfoil

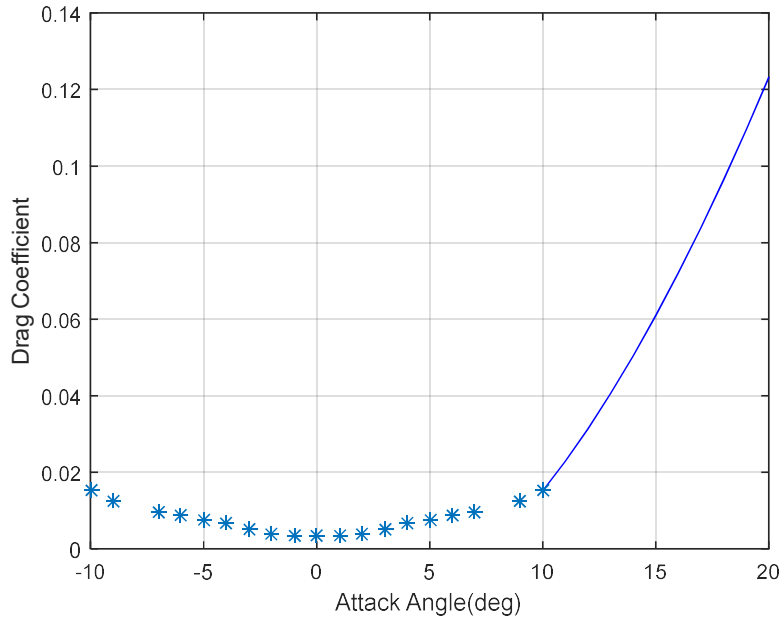


Fig 2.6 2-D drag coefficient data of NACA0012 airfoil

where A_r is the aspect ratio, $C_{L,s}$ is the lift coefficient at stall, $C_{D,s}$ is the drag coefficient at stall and α_s is the stall angle.

The aspect ratio A_r is defined as:

$$A_r = \frac{R}{c_{0.75}} \quad (2.36)$$

The maximum drag coefficient $C_{D,max}$ is calculated by,

$$C_{D,max} = 1.11 + 0.018 A_r \quad A_r \leq 50 \quad (2.37)$$

$$C_{D,max} = 2.01 \quad A_r > 50 \quad (2.38)$$

where $c_{0.75}$ is the chord length at 75 percent radius.

The section lift and drag data predicted from XFOIL and calculated by the stall model are shown in Fig 2.5 and Fig 2.6.

2.3 Comparison with Experiments of other Scholars

Bahaj et al. [33, 98, 101] conducted experiments of a marine current turbine model with 0.8 m diameter in uniform flow in a cavitation channel and a towing tank respectively. In their experiments, the torque and thrust of the turbine were measured. Then the experimental data were compared with several numerical codes.

Using the lift coefficient and drag coefficient presented by Bahaj et al., for pitch angle 10°, results for power coefficients (C_p) and thrust coefficients (C_T) were presented for different tip speed ratios (from 3 to 9) in Fig 2.7 and Fig 2.8. The result shows good agreement, which gives confidence in the classical BEM model we developed for ocean current turbines.

However, to meet with our purpose for design ocean current turbines in shear flow, experiments are necessary to get a new, reliable dataset of the blade loads of ocean current turbine in shear flow, for the development of a robust and fast numerical model.

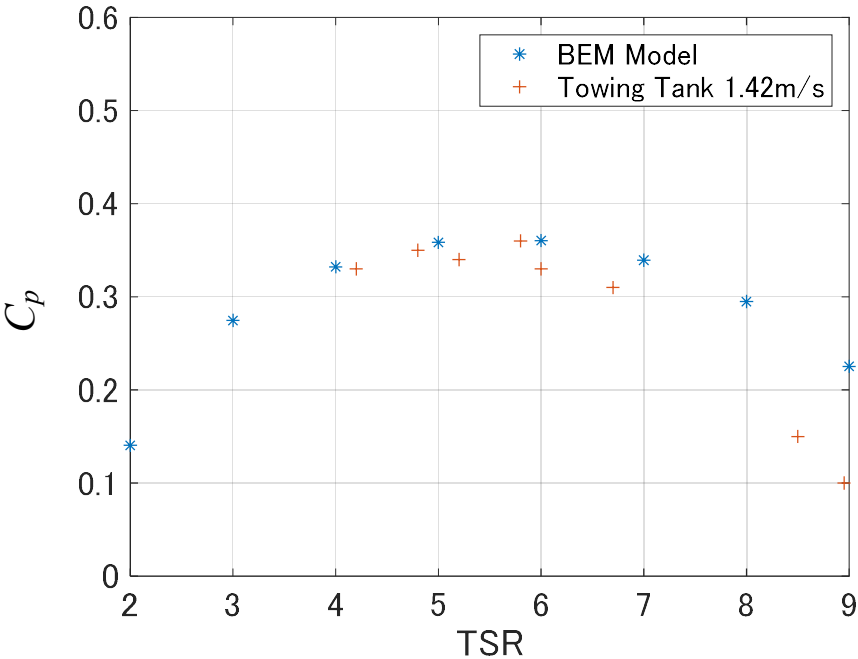


Fig 2.7 Comparison of Power Coefficient- TSR curve with Bahaj’s experiment

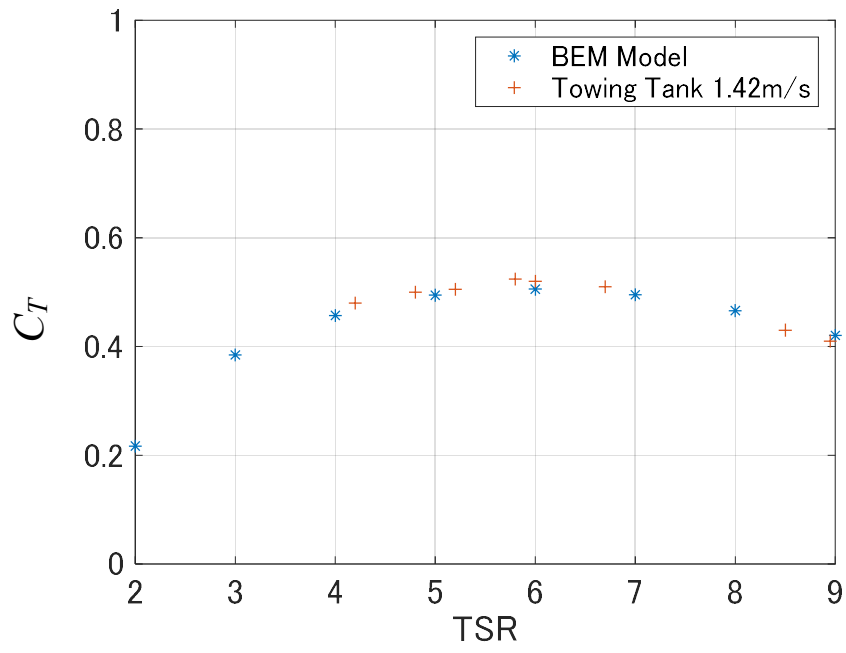


Fig 2.8 Comparison of Thrust coefficient- TSR curve with Bahaj's experiment

3.Experiment and Comparison with the Classical BEM

Establishing methodologies to generate a shear flow in a circulating water channel and to measure the out of plane bending moments at a blade root of the turbine in shear flow is a part of aims of the study. Thus, the shear flow generating screen has been developed, and a measurement system for the bending moments at the blade root is designed and tested. However, the measurement system has limitations, which are described in the appendix, and we gave up to use our data.

The shear flow generating screen and know-hows of our design for the measurement system is used by Yahagi and Takagi [106]. The experimental data obtained by Yahagi and Takagi is used in this thesis for the validation of numerical calculations. Only a summary of the experiment is shown here, and the detail is shown in the appendix.

3.1 Shear Flow Generation

Since only a few researches have been done to generate shear flow in a circulating water channel, we have developed a screen system to generate shear flow and conducted a measurement in the circulating water channel.

There are various devices like rods, screens, perforated plates, honeycombs that have been used by researchers to generate an approximate homogeneous, turbulent shear flow in wind tunnels. Owen and Zienkiewicz [107] reported experimental and mathematical methods to produce the desired velocity profile using a grid of rods in a wind tunnel. Based on the study, Rose [108] designed an experiment to study the turbulence associated with a velocity field corresponding to a uniform mean shear. Champagne and Harris [109] generated an approximately homogeneous turbulent shear flow with a transverse array of channels of equal widths but differing resistance. However, these studies focused on the field of aerodynamics, with all experiments carried out in wind tunnels.

The shear flow profile we designed is according to the observation data in the Kuroshio Current, where the minimum speed in water depth has a 10% deduction compared with the highest flow speed in the water depth. Although the actual flow does not decay linearly in depth, it is perfectly fine to develop a scheme that takes into consideration the linear gradient of the vertical velocity to reproduced the linear component of the vertical shear of the Kuroshio Current. Based on the theory by Owen & Zienkiewicz [107] and Corrsin [110], a three-screen system has been developed. An example of the approximately linear shear profile is shown in Fig. 3.1.

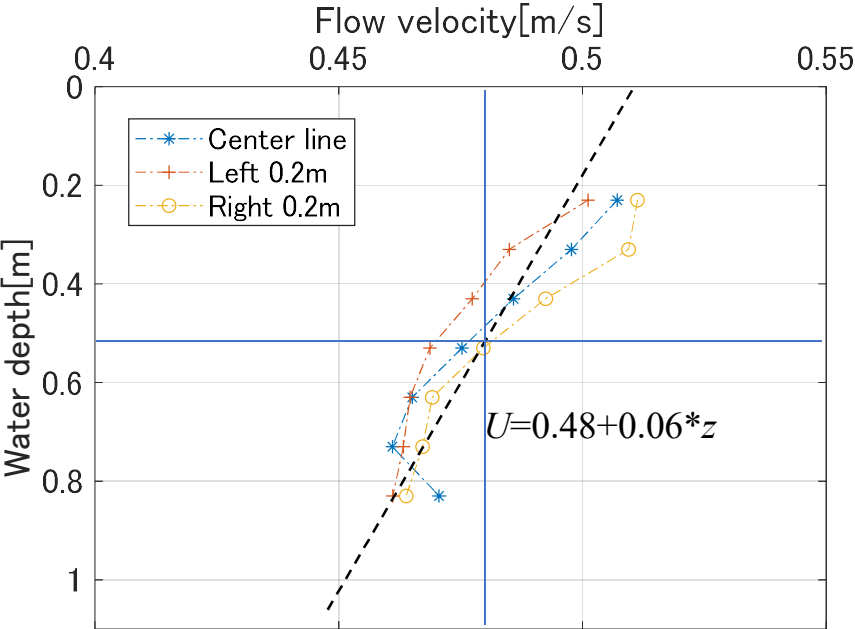


Fig 3.1 Shear flow profile with water depth generated by the three screen system

The size of measurement section of the circulating water channel is shown in Table 3.1.

Table 3.1 Size parameters of the circulating water tank

Total depth	1.4m
Water depth	1.1m- 1.2m
Width	1.71m

Yahagi and Takagi [106] used the same screen system to generate the shear flow in the circulating water channel of Akishima Laboratories Inc., and the shear flow profile is shown in Fig. 3.2, which shows a more linear profile.

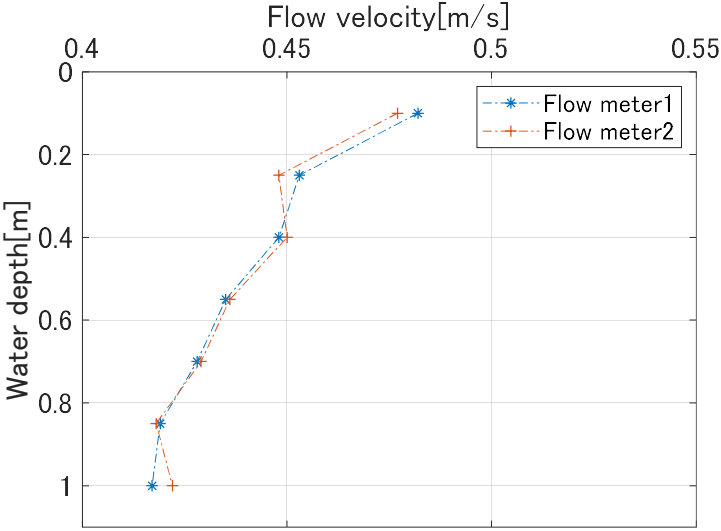


Fig 3.2 Shear flow profile with water depth generated by the three screen system in the circular water channel of Akishima Laboratories Inc.

3.2 Model Turbine and Measurement

A rotor diameter of 0.88m (1/50 scale) was selected to maximize Reynolds number with low blockage ratio in the circulating water channel. The sectional shape of blades is NACA0012. The model blades were made from aluminum for accuracy.

The rotor hub has 0.12 m diameter and has two removable bolts that fix each blade, which makes it possible to change the blade pitch angle. Three pitch angles, i.e. -2 degree, 0 degree and 2 degree, are adopted in the measurement. A supporting frame that could be fixed in both the circulating water channel and the carriage of the towing tank was designed. A two-component load cell is equipped to measure the out of plane bending moments and in plane bending moments at one blade root. There is also a torque sensor to measure the torque. The overall turbine design is shown in Fig 3.3.

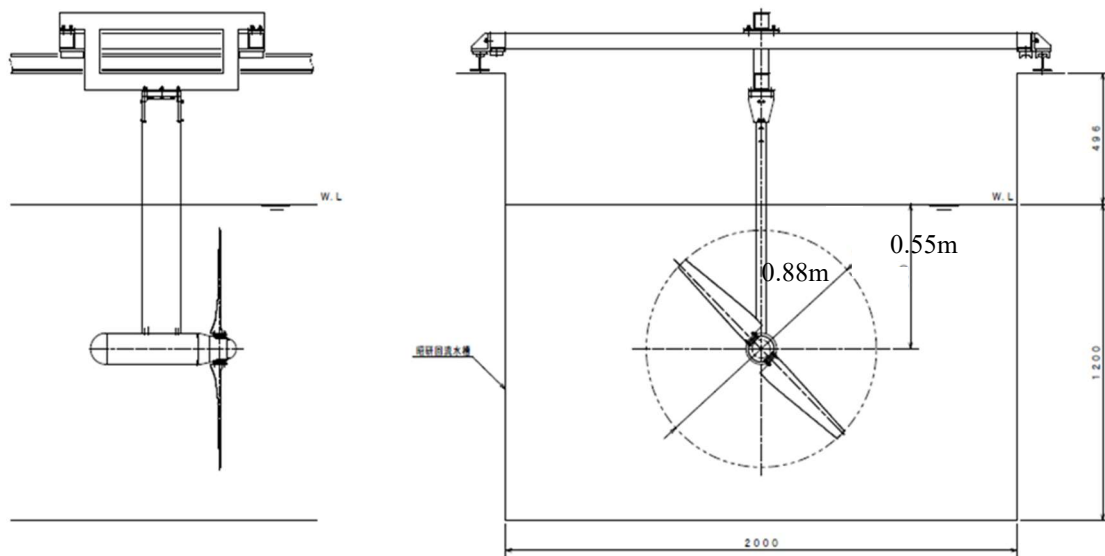


Fig 3.3 Side and front view of experimental turbine

To get the blockage coefficient and the free surface correction, the same model turbine is tested in the towing tank in the Chiba experimental station of the University of Tokyo. The towing tank has a length of 50 m, width of 10 m and depth of 5 m. In the towing tank, the rotor

was centered at 0.2 m below the water surface. The blockage rate in the towing tank is 1.2%. Experimental results from the circulating water channel have been corrected for blockage using the model by Batten et al. [56].

All measured values are non-dimensionalized by using the following definitions.

$$TSR = \frac{\Omega R}{U_0} \quad (3.1)$$

$$C_p = \frac{Q\Omega}{0.5\rho AU_0^3} \quad (3.2)$$

$$C_T = \frac{T}{0.5\rho AU_0^2} \quad (3.3)$$

$$C_{my} = \frac{M_y}{0.5\rho A U_0^2} \quad (3.4)$$

where Ω is averaged rotation speed (rad/s), R is the rotor radius (m), U_0 is the free stream velocity at turbine hub center (m/s) and ρ is the fluid density (kg/m³), M_y is the out of plane bending moment at the blade root of ocean current turbines (N*m), A is the swept area(m²).

Since the measured value in shear flow has a periodic fluctuation, the flapwise bending moment coefficient is expressed as a linear superposition of a fluctuating component and the mean value:

$$C_{my}(t) = C_{my_a} \cos(\Omega t + \theta_{C_{my}}) + C_{my_m} \quad (3.5)$$

where Ω is the angular velocity of the rotor, C_{my_a} is the amplitude of flapwise bending moment coefficient, C_{my_m} is the averaged flapwise bending moment coefficient, while $\theta_{C_{my}}$ is the phase angle of flapwise bending moment coefficient.

3.3 Comparison with Classical BEM Model

3.3.1 Performance Comparison

The results of the performance of the ocean current turbine model calculated with the classical BEM model has been compared with experimental data by Yahagi and Takagi [144].

The comparisons between the classical BEM results and Yahagi's experiment results for power coefficients and thrust coefficients are depicted in Fig 3.4 and Fig 3.5, respectively, pitch angle -2° and 0° .

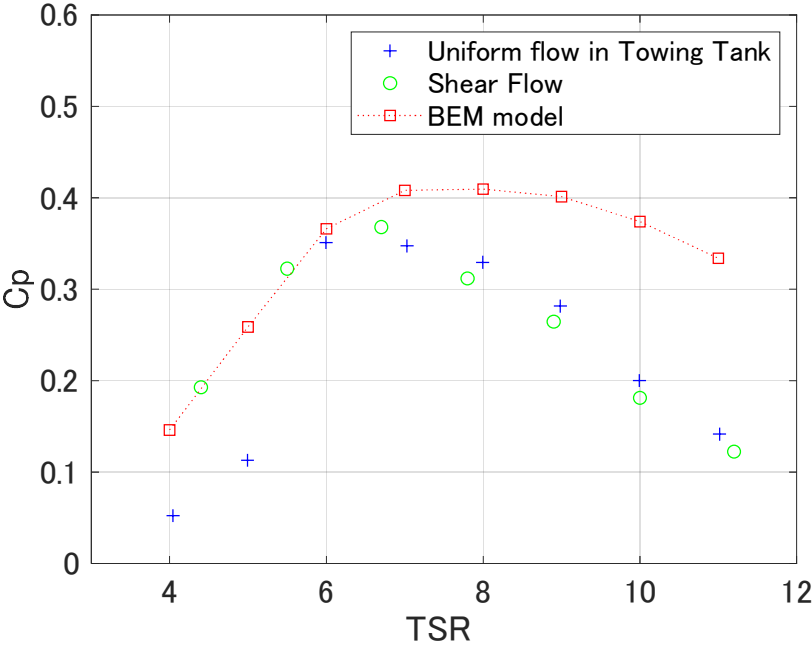


Fig 3.4a Comparison of power coefficients with *TSR* when pitch angle is -2°

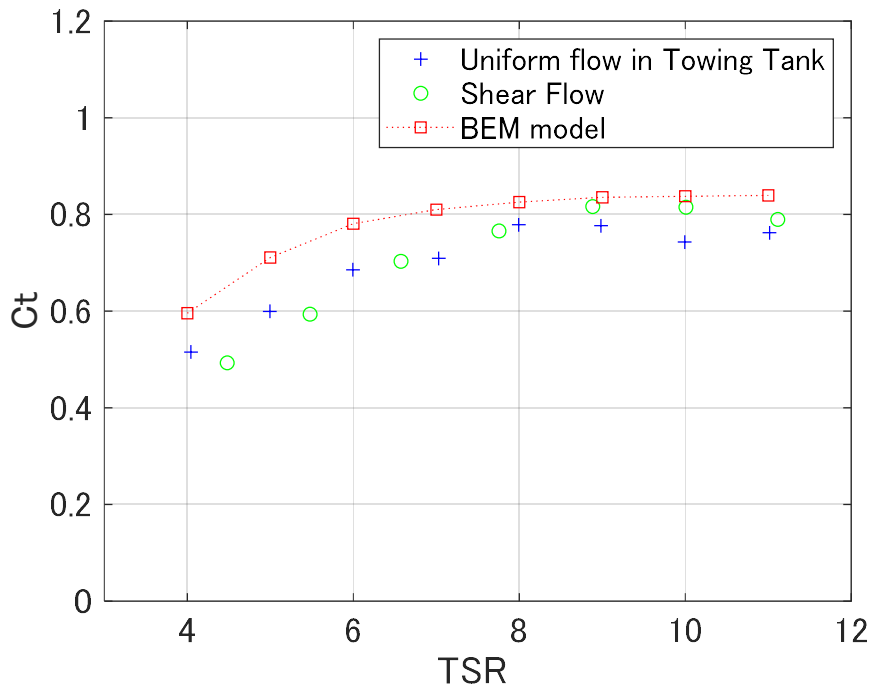


Fig 3.4b Comparison of thrust coefficients with TSR when pitch angle is -2°

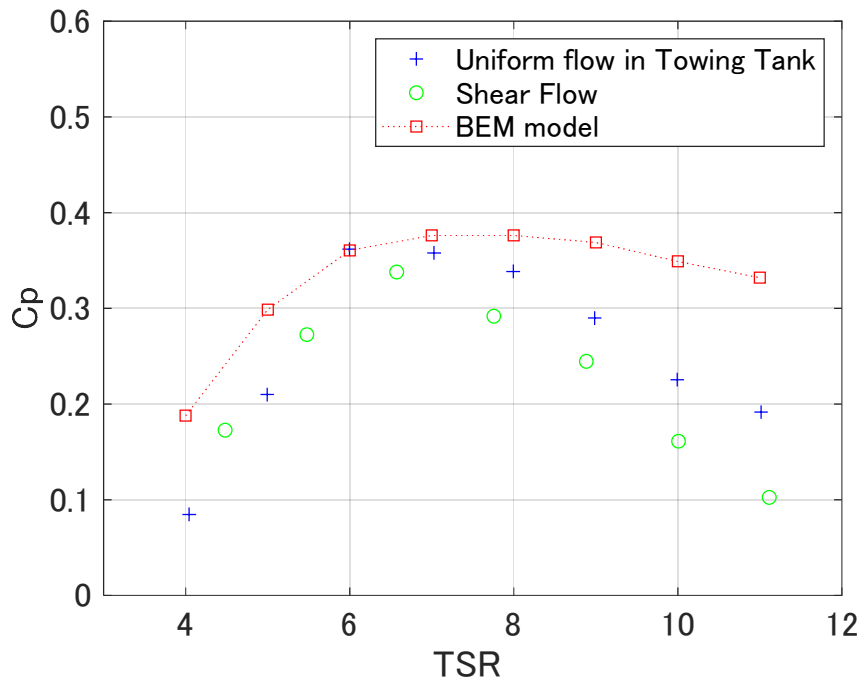


Fig 3.5a Comparison of power coefficients with TSR when pitch angle is 0°

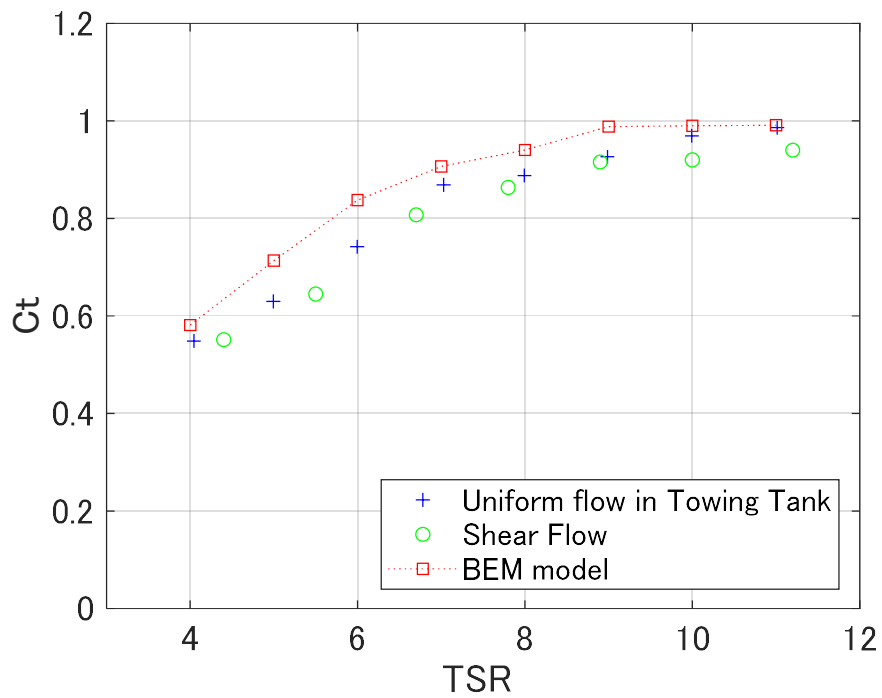


Fig 3.5b Comparison of thrust coefficients with TSR when pitch angle is 0°

In general, results are in good agreement with the experimental results. For low and high TSR , the classical BEM model tends to overestimate the power coefficients. The reason of overestimation is discussed in Section 5.4.

3.3.2 Bending moment comparison

Giving a linear profile of inflow velocity in z-direction, we calculate blade bending moment with classical BEM theory. The calculated results of the averaged flapwise bending moment are compared with Yahagi's experimental results in Fig 3.6 both for the uniform flow and the shear flow. The classical BEM model can predict the averaged flapwise bending moment satisfactory as shown in Fig 3.6.

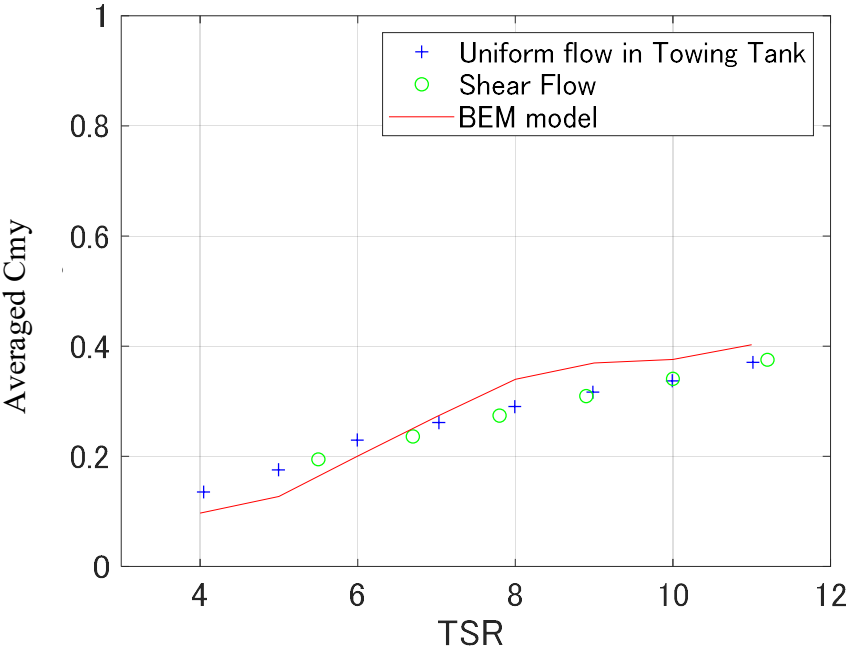


Fig 3.6a Comparison of averaged flapwise bending moment coefficients when pitch angle is -2°

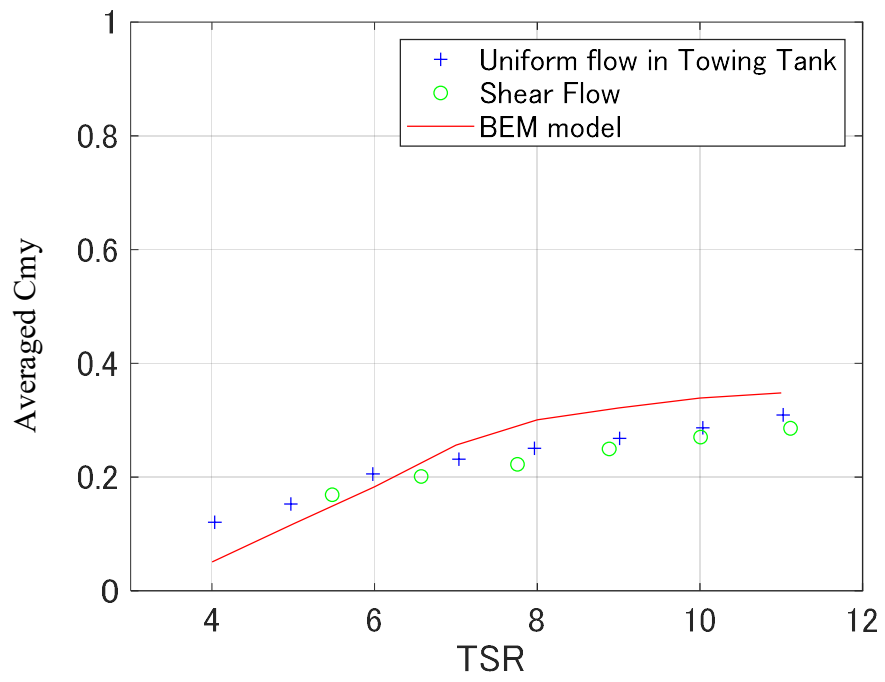


Fig 3.6b Comparison of averaged flapwise bending moment coefficients when pitch angle is 0°

Chapter 4-5 (pp. 66 to 133) of my doctoral thesis cannot be made public on the Internet for 5 years from the date of doctoral degree conferral because that part is to be published in journal papers.

6. Summary and Conclusion

The floating ocean current turbine has been proposed as a new way to harness the current energy. Japan has piloted on the field ocean current turbine by the concept design and field tests. It is expected that the research work on ocean current turbines will help to develop the industry of the ocean energy generation, which will make a contribution to the higher energy security of Japanese society.

For the marine current turbine, including ocean current turbine and tidal current turbine, most of the technology is from the study of the wind turbine which has clear international standards and commercial software. There are some differences in thrust, aspect ratio and solidity between tidal current turbines and wind turbines. In addition, a shear profile of flow near the sea surface is different. Shear flow is a significant challenge to the ocean current turbine because it could cause fluctuations in the inflow of the blades and altered the bending moments on the blade roots of the ocean current turbine. Moreover, little study has been made on the study and experiment of hydrodynamic shear flow.

A new BEM model combined with Theodorsen's function to represent the unsteadiness of the blade force has been proposed and series of numerical simulations with the classical BEM and the new BEM model have been conducted. Major conclusions are described in the following sections.

6.1 BEM Model

In practice, seldom is the case that only the classical BEM theory is used for the calculation or design of turbine blades. As for the tidal current turbines, several principal corrections were applied with the original BEM theory to improve the accuracy. The corrections include tip loss correction and hub loss correction, thrust correction and correction after stall.

We have compared with the experiments of other scholars, and the results show good agreements. Through the comparisons with our experimental results in uniform flow, it is found that the accuracy of the original BEM theory has been greatly improved with several corrections and it is satisfactory for application to the motion simulation, while overestimating the power coefficient at high tip speed ratios has been observed. However, we showed a possibility that it is caused by the underestimation of drag coefficients in XFOil and it could be improved by utilizing the measured data.

The effect of shear flow on structural loading is important, since the shear flow can lead to fluctuations in bending moments. The classical BEM model overestimates the amplitudes of the fluctuations in the out of plane bending moment at the blade root. This shows the classical BEM should be greatly improved on the accuracy of the load prediction with a simple and non-time consuming numerical method.

6.2 Unsteady Theory

The mathematical models of the unsteady thin airfoil theory have been reviewed and an unsteady BEM theory as a simple numerical simulation method for the design of blade performance of horizontal axis ocean current turbines has been established combining Theodorsen's function with the classical BEM theory.

The results show that simulation results are improved compared to classical BEM theory, when the out of plane bending moments at the blade root of ocean current turbines in shear flow are calculated. It is confirmed that the accuracy of classical BEM theory to predict hydrodynamic loads in shear flow is enhanced by adding the unsteady effect represented by Theodorsen's function.

Loewy's function which considers returning wakes is also tested as another candidate for representing the unsteady effect. However, it is found that the difference between

Theodorsen's function and Loewy's function is negligible. This means that the effects of the other layers of trailing vortex, i.e. helical trailing vortex are negligible.

In order to validate the numerical model, we have established the three screen system to generate shear flow in a circulating water channel. A two-bladed horizontal axis turbine which is uniquely used for the ocean current power generation was used to measure not only the torque but also the out of plane bending moments at one blade root, and measurement system has been developed. However, the experimental results were not satisfactory because of the brake system which present a torque moment. Thus we used different experimental results.

Through the comparisons with experimental results and parametric calculation, it is confirmed that the classical BEM theory combined with Theodorsen's function can offer a satisfactory prediction for the unsteady condition for ocean current turbines as a simple and fast calculation method which can be easily utilized to a motion simulator.

6.3 Important Factors for Accuracy of the Results

We have also found several important factors that affect the accuracy of the hydrodynamic load prediction of ocean current turbines.

Generally speaking, the attack angle increases with the decrease of tip speed ratios. The stall happens at a low tip speed ratio, thus the accuracy of stall model is of importance when the tip speed ratio is low. The range in which stall happens is illustrated for typical tip speed ratios and blade pitch angles.

Tip loss correction is also significant for ocean current turbines. It is found that the tip loss model affects the induction factors of blade sections near the blade tip, thus the influence on the out of plane bending moment at the blade root is significant in most

calculations, while influence on the tangential induction factor is negligible and effect of the hub loss is not significant.

For the drag coefficient calculated from Xfoil, it is found that the drag coefficient affects the power coefficients for two-bladed ocean current turbine, especially for high tip speed ratios.

We have also calculated the case of high shear gradient and compared with CFD results. In the high shear gradient case, the fluctuation of the out of plane bending moments is in good agreement with the CFD results. Thus the new BEM model is valid in the high shear case. It is found that the local attack angle distribution in BEM results shows tendency of dynamic stall in the CFD calculations in the high shear gradient.

Summarizing the results obtained in this thesis, it is concluded that the combined BEM with Theodorsen's theory presents a simple and fast method for calculating the turbine blade load in shear flow. The accuracy of the proposed method is not perfect. However, the accuracy of unsteady load estimation by the new method has been apparently improved compared to the classical BEM.

In the realistic design of an ocean current turbine, the basic performances of the turbine such as the power coefficient and the thrust coefficient are supposed to be estimated by the CFD or the direct measurement. On the other hand, long term statistical values such as the fatigue life of the blade and the mooring line are estimated by the motion simulator which does not incorporate unsteady blade load model. The unsteady blade model has apparently required less computational resources, because the long-term prediction takes long time to calculate the all design cases required for the turbine design. Therefore, the present method must be one of promising mathematical models for updating the motion simulator.

In order to incorporate the present method, the code should be adapted to the time domain simulation, and further improvement of accuracy should be pursued according to suggestions mentioned in the previous chapter. These are the future works.

Acknowledgement

This thesis was completed under the guidance of my supervisor, Professor Ken Takagi. Professor Takagi's profound professional knowledge and serious scientific attitude motivated me a lot. When I had problems in experiments and simulation, he always shared his ideas with great patience to me although he is fully occupied. I really appreciate his kindness.

I would like to show great gratitude also to every professor in my defense committee, they have come up with many insights and their suggestions are of importance to overcome the difficulties in the thesis.

The experiments were supported by the New Energy and Industrial Technology Development Organization (NEDO) and IHI Corporation, I would like to show my appreciation to them.

From the selection of the subject, Dr. Ryota Wada and Dr. Keiji Kiyomatsu have always given me detailed guidance and advice. In the experiments, my lab members and Researcher Yoshida and other researchers in the Chiba station have offered great help. I can't finish the experiments without them. I would like to extend my sincere gratitude to them.

For the kindness and help of Takagi lab members and Waseda lab members in life and study, I can't thank everyone enough.

I want to thank my friends in Japan and in China, they helped me get through hard times in life.

Thanks to my company, ECOH Corporation, especially for Dr. Hideyuki Shibaki and my department members, for every support and encouragement, which made a big difference.

Finally, I would also like to thank my parents, my family, who are always standing by me.

References

- 1) Agreement P. United nations framework convention on climate change[J]. Paris, France, 2015.
- 2) Zhang C, Chen H P. Optimum Maintenance Strategy for Fatigue Damaged Composite Blades of Offshore Wind Turbines using Stochastic Modelling[J].
- 3) Stolpe M, Buhl T, Sumer B M, et al. Offshore wind energy developments[M]//Dtu International Energy Report 2014. Technical University of Denmark (DTU), 2014: 43-51.
- 4) Bhattacharya S. Challenges in design of foundations for offshore wind turbines[J]. Engineering & Technology Reference, 2014, 1(1): 922.
- 5) Veritas, B. Classification and Certification of Floating Offshore Wind Turbines. Guidance Note NI572, 2010
- 6) Esteban M, Leary D. Current developments and future prospects of offshore wind and ocean energy[J]. Applied Energy, 2012, 90(1): 128-136.
- 7) Henderson A R, Witcher D. Floating offshore wind energy—a review of the current status and an assessment of the prospects[J]. Wind Engineering, 2010, 34(1): 1-16.
- 8) Stiesdal, H. Hywind: The world's first floating MW-scale wind turbine. Wind Directions, 2009, 31, 52-53.
- 9) Sun X, Huang D, Wu G. The current state of offshore wind energy technology development[J]. Energy, 2012, 41(1): 298-312.
- 10) Elghali S E B, Benbouzid M E H, Charpentier J F. Marine tidal current electric power generation technology: State of the art and current status[C]//Electric Machines & Drives Conference, 2007. IEMDC'07. IEEE International. IEEE, 2007, 2: 1407-1412.
- 11) Khan M J, Bhuyan G, Iqbal M T, et al. Hydrokinetic energy conversion systems and assessment of horizontal and vertical axis turbines for river and tidal applications: A technology status review[J]. Applied energy, 2009, 86(10): 1823-1835.
- 12) Hagerman G, Polagye B, Bedard R, et al. Methodology for estimating tidal current energy resources and power production by tidal in-stream energy conversion (TISEC) devices[J]. EPRI North American tidal in stream power feasibility

- demonstration project, 2006, 1.
- 13) Kumar V S, Dora G U, Philip S, et al. Variations in tidal constituents along the nearshore waters of Karnataka, west coast of India[J]. *Journal of Coastal Research*, 2010, 27(5): 824-829.
 - 14) Nicholls-Lee R F, Turnock S R. Tidal energy extraction: renewable, sustainable and predictable[J]. *Science Progress*, 2008, 91(1): 81-111.
 - 15) ETSU. Tidal stream energy review. Technical report ETSU-T05/00155/REP, Harwell Laboratory, Energy Technology Support Unit, DTI, 1993
 - 16) Fraenkel P L. Power from marine currents[J]. *Proceedings of the Institution of Mechanical Engineers, Part A: Journal of Power and Energy*, 2002, 216(1): 1-14.
 - 17) Batten W M J, Bahaj A S, Molland A F, et al. Experimentally validated numerical method for the hydrodynamic design of horizontal axis tidal turbines[J]. *Ocean engineering*, 2007, 34(7): 1013-1020.
 - 18) Bahaj A S, Myers L E, Thomson M D, et al. Characterising the wake of horizontal axis marine current turbines[C]//*Proceedings of the 7th European wave and tidal energy conference*. University of Southampton Porto, Portugal, 2007: 9.
 - 19) Callaghan, J. Future marine energy: results of the marine energy challenge: cost competitiveness and growth of wave and tidal stream energy, Carbon Trust, 2006
 - 20) Rourke F O, Boyle F, Reynolds A. Marine current energy devices: current status and possible future applications in Ireland[J]. *Renewable and Sustainable Energy Reviews*, 2010, 14(3): 1026-1036.
 - 21) Bahaj A B S. Generating electricity from the oceans[J]. *Renewable and Sustainable Energy Reviews*, 2011, 15(7): 3399-3416.
 - 22) Zhang J, Moreau L, Machmoum M, et al. State of the art in tidal current energy extracting technologies[C]//*Green Energy, 2014 International Conference on*. IEEE, 2014: 1-7.
 - 23) Ng K W, Lam W H, Ng K C. 2002–2012: 10 years of research progress in horizontal-axis marine current turbines[J]. *Energies*, 2013, 6(3): 1497-1526.
 - 24) <https://tethys.pnnl.gov/annex-iv-sites/openhydro-alderney>
 - 25) <http://www.andritzhydrohammerfest.co.uk/tidal-turbines/>
 - 26) <https://tethys.pnnl.gov/annex-iv-sites/strangford-lough-mct-seagen>

- 27) <https://phys.org/news/2012-05-scotland-turbine-harness-tidal-power.html>
- 28) <https://www.treehugger.com/renewable-energy/tidel-harnesses-lunar-energy.html>
- 29) https://tethys.pnnl.gov/sites/default/files/publications/Stingray_Tidal_Stream_Energy_Device.pdf
- 30) http://www.emec.org.uk/about-us/media-centre/gallery/installation-of-voith-turbine-at-emec-tidal-test-site-credit-voith-img_2416/
- 31) <http://www.sabella-d10.bzh/>
- 32) Pelc R, Fujita R M. Renewable energy from the ocean[J]. *Marine Policy*, 2002, 26(6): 471-479.
- 33) https://www.adp.noaa.gov/currents_map.html
- 34) http://www.nedo.go.jp/news/press/AA5_100824.html
- 35) 2005 IEEE Power Engineering Society General Meeting Panel Session, Harnessing the untapped energy potential of the oceans: Tidal, wave, currents and OTEC, San Francisco (USA), June 2005.
- 36) Myers L, Bahaj A S. Power output performance characteristics of a horizontal axis marine current turbine[J]. *Renewable energy*, 2006, 31(2): 197-208.
- 37) Bahaj A S, Myers L E. Fundamentals applicable to the utilisation of marine current turbines for energy production[J]. *Renewable energy*, 2003, 28(14): 2205-2211.
- 38) <https://simecatlantis.com/>
- 39) <https://www.nasa.gov/topics/earth/features/perpetual-ocean.html>
- 40) Kiyomatsu K, Kodaira T, Waseda T, et al. Validation of ocean current and power near Miyake Island. [J]. *Journal of the Japan Society of Naval Architects and Ocean Engineers*, 2014, 19.
- 41) Kiyomatsu K, Kodaira T, Kadomoto Y, et al. ADCP measurements of ocean currents near Miyake Island[J]. *Journal of the Japan Society of Naval Architects and Ocean Engineers*, 2014, 20.
- 42) Makino K, Takagi K, Waseda T, et al. Reproduction of velocity time series for designing the ocean current turbine[C]//*Oceans-St. John's*, 2014. IEEE, 2014: 1-6.
- 43) Xia Y, Takagi K. Effect of shear flow on a marine current turbine[C]//*OCEANS 2016-Shanghai*. IEEE, 2016: 1-5.
- 44) Viterna L A, Corrigan R D. Fixed pitch rotor performance of large horizontal axis wind turbines[J]. 1982.

- 45) Kiefer J, Miller M A, Hultmark M, et al. Effects of finite aspect ratio on wind turbine airfoil measurements[C]//Journal of Physics: Conference Series. IOP Publishing, 2016, 753(2): 022040.
- 46) Kumar R, Baredar P. Solidity Study and its Effects on the Performance of A Small Scale Horizontal Axis Wind Turbine[J]. Energy Centre, Maulana Azad National Institute of Technology, Bhopal, Madhya Pradesh, India, 462051.
- 47) Menet J L. A double-step Savonius rotor for local production of electricity: a design study[J]. Renewable energy, 2004, 29(11): 1843-1862.
- 48) Dai J C, Hu Y P, Liu D S, et al. Aerodynamic loads calculation and analysis for large scale wind turbine based on combining BEM modified theory with stall model[J]. Renewable Energy, 2011, 36(3): 1095-1104.
- 49) Tahani M, Kavari G, Masdari M, et al. Aerodynamic design of horizontal axis wind turbine with innovative local linearization of chord and twist distributions[J]. Energy, 2017, 131: 78-91.
- 50) Vaz J R P, Pinho J T, Mesquita A L A. An extension of BEM method applied to horizontal-axis wind turbine design[J]. Renewable Energy, 2011, 36(6): 1734-1740.
- 51) Glauert, H. The analysis of experimental results in the windmill brake and vortex ring states of an airscrew, HM Stationery Office, 1926
- 52) Spera D A. Wind turbine technology[J]. 1994.
- 53) Buhl Jr M L. New empirical relationship between thrust coefficient and induction factor for the turbulent windmill state[R]. National Renewable Energy Lab.(NREL), Golden, CO (United States), 2005.
- 54) Shen W Z, Mikkelsen R, Sørensen J N, et al. Tip loss corrections for wind turbine computations[J]. Wind Energy: An International Journal for Progress and Applications in Wind Power Conversion Technology, 2005, 8(4): 457-475.
- 55) Sun X, Chick J P, Bryden I G. Laboratory-scale simulation of energy extraction from tidal currents[J]. Renewable Energy, 2008, 33(6): 1267-1274.
- 56) Batten, WMJ, Blunden, LS, Bahaj, AS. CFD simulation of a small farm of horizontal axis marine current turbines, Proceedings World Renewable Energy Congress (WREC) VIII, Florence, pp 19-25, 2006
- 57) Clarke J A, Connor G, Grant A D, et al. Design and testing of a contra-rotating tidal current turbine[J]. Proceedings of the Institution of Mechanical Engineers,

- Part A: Journal of Power and Energy, 2007, 221(2): 171-179.
- 58) Masters I, Chapman J C, Willis M R, et al. A robust blade element momentum theory model for tidal stream turbines including tip and hub loss corrections[J]. Journal of Marine Engineering & Technology, 2011, 10(1): 25-35.
 - 59) DNV GL Garrad Hassan. Tidal Bladed Theory Manual, 2012
 - 60) McCann G N. Tidal current turbine fatigue loading sensitivity to waves and turbulence—a parametric study[C]//Proceedings of the 7th European Wave and Tidal Energy Conference. 2007.
 - 61) “The exploitation of tidal marine currents (non-nuclear energy JOULE II project results),” Report EUR 16683EN, DG Science, Research and Development, The European Commission Office for Official Publications, Luxembourg, 1996.
 - 62) Myers L, Bahaj A S. Wake studies of a 1/30th scale horizontal axis marine current turbine[J]. Ocean Engineering, 2007, 34(5-6): 758-762.
 - 63) Bahaj A S, Molland A F, Chaplin J R, et al. Power and thrust measurements of marine current turbines under various hydrodynamic flow conditions in a cavitation tunnel and a towing tank[J]. Renewable energy, 2007, 32(3): 407-426.
 - 64) Ponta F L, Jacovkis P M. Marine-current power generation by diffuser-augmented floating hydro-turbines[J]. Renewable energy, 2008, 33(4): 665-673.
 - 65) Wang J, Müller N. Performance prediction of array arrangement on ducted composite material marine current turbines (CMMCTs)[J]. Ocean engineering, 2012, 41: 21-26.
 - 66) Finkl C W, Charlier R. Electrical power generation from ocean currents in the Straits of Florida: Some environmental considerations[J]. Renewable and Sustainable Energy Reviews, 2009, 13(9): 2597-2604.
 - 67) Lee S H, Lee S H, Jang K, et al. A numerical study for the optimal arrangement of ocean current turbine generators in the ocean current power parks[J]. Current Applied Physics, 2010, 10(2): S137-S141.
 - 68) Luquet R, Bellevre D, Fréchou D, et al. Design and model testing of an optimized ducted marine current turbine[J]. International journal of marine energy, 2013, 2: 61-80.
 - 69) Carpenter, P. J., and Fridovich, B., “Effect of A Rapid Blade-Pitch Increase on the Thrust and Induced-Velocity Response of a Full-Scale Helicopter Rotor,” NACA TN 3044, Nov. 1953.
 - 70) Pitt, D. M., and Peters, D. A., “Rotor Dynamic Inflow Derivatives and Time Constants from Various Inflow Models,” 9th European Rotorcraft Forum, Stresa,

Italy, Sept. 13–15, 1983.

- 71) Peters, D. A., “Hingeless Rotor Frequency Response with Unsteady Aerodynamics,” AHS/NASA Specialists’ Meeting on Rotorcraft Dynamics, NASA SP-362, 1974.
- 72) Peters, D. A., Karunamoorthy, S., and Cae, W.-M., “Finite State Induced Flow Models Part I: Two Dimensional Thin Airfoil,” *Journal of Aircraft*, Vol. 32, No. 2, 1995, pp. 313–322.
- 73) Peters, D. A., and He, C. J., “Finite State Induced Flow Models Part II: Three-Dimensional Rotor Disk,” *Journal of Aircraft*, Vol. 32, No. 2, 1995, pp. 323–333.
- 74) Hansen M O L. *Aerodynamics of wind turbines*[M]. Routledge, 2015.
- 75) Bierbooms, W., “A Comparison Between Unsteady Aerodynamic Models,” *Proceedings of the European Wind Energy Conference*, Amsterdam, The Netherlands, 1991.
- 76) Snel H, Schepers J G. *Joint investigation of dynamic inflow effects and implementation of an engineering method*[M]. Netherlands Energy Research Foundation ECN, 1995.
- 77) Clark, D. R., and Leiper, A. C., “The Free Wake Analysis– A Method for Prediction of Helicopter Rotor Hovering Performance,” *Journal of the American Helicopter Society*, Vol. 15, No. 1, Jan. 1970, pp. 3–11.
- 78) Leishman G J. *Principles of helicopter aerodynamics with CD extra*[M]. Cambridge university press, 2006.
- 79) Wagner, H., “Über die Entstehung des dynamischen Auftriebes von Tragflügel,” *Febru- ary 1925*, pp. 17–35.
- 80) Theodorsen T. *General theory of aerodynamic instability and the mechanism of flutter*[J]. NACA Technical Report, 1935 (496).
- 81) Küssner, H. G., “Zusammenfassender Bericht über den instationären Auftrieb von Flügel,” *December 1936*, pp. 410–424., H. G., “Zusammenfassender Bericht über den instationären Auftrieb von Flügel,” *December 1936*, pp. 410–424.
- 82) von Kármán, Th., and Sears, W.R., “Airfoil Theory for Non-Uniform Motion,” *Journal of the Aeronautical Sciences*, Vol. 5, No. 10, 1938, pp. 379–390.
- 83) Bhagwat, M. J., and Leishman, J. G., “Stability Analysis of Rotor Wakes in Axial

- Flight,” *Journal of the American Helicopter Society*, Vol. 45, No. 3, 2000.
- 84) Leishman J G. Challenges in modelling the unsteady aerodynamics of wind turbines[J]. *Wind Energy: An International Journal for Progress and Applications in Wind Power Conversion Technology*, 2002, 5(2 - 3): 85-132.
- 85) Sears, W., “Operational Methods in the Theory of Airfoils in Nonuniform Motion,” *Journal of the Franklin Institute*, Vol. 230, 1940, pp. 95–111.
- 86) Garrick, I. E., “On Some Reciprocal Relations in the Theory of Nonstationary Flows,” *NACA TR No. 629*, March 1938.
- 87) Loewy, R.G., 1957, “A Two-dimensional Approximation to the Unsteady Aerodynamics of Rotary Wings”, *J. Aeronaut. Sci.* Vol. 24, No 2, pp 81-92.
- 88) Maganga F, Germain G, King J, et al. Experimental study to determine flow characteristic effects on marine current turbine behaviour[C]//EWTEC 2009, Uppsala. 2009.
- 89) Barltrop N, Varyani K S, Grant A, et al. Wave-current interactions in marine current turbines[J]. *Proceedings of the Institution of Mechanical Engineers, Part M: Journal of Engineering for the Maritime Environment*, 2006, 220(4): 195-203.
- 90) Galloway P W, Myers L E, Bahaj A S. Studies of a scale tidal turbine in close proximity to waves[J]. 2010.
- 91) Milne I. An experimental investigation of turbulence and unsteady loading on tidal turbines[D]. *ResearchSpace@ Auckland*, 2013.
- 92) Milne I A, Day A H, Sharma R N, et al. Blade loads on tidal turbines in planar oscillatory flow[J]. *Ocean Engineering*, 2013, 60: 163-174.
- 93) Carlton J. *Marine propellers and propulsion*[M]. Butterworth-Heinemann, 2012.
- 94) Burton T, Jenkins N, Sharpe D, et al. *Wind energy handbook*[M]. John Wiley & Sons, 2011.
- 95) Branlard E, Dixon K, Gaunaa M. An improved tip-loss correction based on vortex code results[J]. *Proceedings, EWEA-The European Wind Energy Association*, 2012.
- 96) Moriarty P J, Hansen A C. *AeroDyn theory manual*[M]. Golden, CO: National Renewable Energy Laboratory, 2005.
- 97) Glauert H. *Airplane propellers*[M]//*Aerodynamic theory*. Springer, Berlin, Heidelberg, 1935: 169-360.

- 98) Batten W M J, Bahaj A S, Molland A F, et al. The prediction of the hydrodynamic performance of marine current turbines[J]. *Renewable energy*, 2008, 33(5): 1085-1096.
- 99) <https://wind.nrel.gov/airfoils/AirfoilData.html>
- 100) https://m-selig.ae.illinois.edu/ads/coord_database.html
- 101) Bahaj AS, Myers LE. Cavitation prediction in operating marine current turbines. Proceedings of conference C67 of the solar energy society, Belfast; 2001.
- 102) Drela M. XFOIL: An analysis and design system for low Reynolds number airfoils[M]//*Low Reynolds number aerodynamics*. Springer, Berlin, Heidelberg, 1989: 1-12.
- 103) Song M, Kim M C, Do I R, et al. Numerical and experimental investigation on the performance of three newly designed 100 kW-class tidal current turbines[J]. *International Journal of Naval Architecture and Ocean Engineering*, 2012, 4(3): 241-255.
- 104) Abbott I H, Von Doenhoff A E. Theory of wing sections, including a summary of airfoil data[M]. Courier Corporation, 1959.
- 105) Molland A F, Bahaj A S, Chaplin J R, et al. Measurements and predictions of forces, pressures and cavitation on 2-D sections suitable for marine current turbines[J]. *Proceedings of the Institution of Mechanical Engineers, Part M: Journal of Engineering for the Maritime Environment*, 2004, 218(2): 127-138.
- 106) Yahagi, K., & Takagi, K. (2019). Moment loads acting on a blade of an ocean current turbine in shear flow. *Ocean Engineering*, 172, 446-455.
- 107) Owen P R, Zienkiewicz H K. The production of uniform shear flow in a wind tunnel[J]. *Journal of Fluid Mechanics*, 1957, 2(6): 521-531.
- 108) Rose W G. Results of an attempt to generate a homogeneous turbulent shear flow[J]. *Journal of fluid mechanics*, 1966, 25(1): 97-120.
- 109) Champagne F H, Harris V G, Corrsin S. Experiments on nearly homogeneous turbulent shear flow[J]. *Journal of Fluid Mechanics*, 1970, 41(1): 81-139.
- 110) Corrsin S. Estimates of the relations between Eulerian and Lagrangian scales in large Reynolds number turbulence[J]. *Journal of the Atmospheric Sciences*, 1963, 20(2): 115-119.
- 111) Yahagi, K and Takagi, K., Personal communication.
- 112) Cetin, N. S., Yurdusev, M. A., Ata, R., & Ozdemir, A. (2005). Assessment of

- optimum tip speed ratio of wind turbines. *Mathematical and Computational Applications*, 10(1), 147-154.
- 113) Ragheb, M., & Ragheb, A. M. (2011). Wind turbines theory-the betz equation and optimal rotor tip speed ratio. In *Fundamental and advanced topics in wind power*. InTech.
- 114) Song, M., Kim, M. C., Do, I. R., Rhee, S. H., Lee, J. H., & Hyun, B. S. (2012). Numerical and experimental investigation on the performance of three newly designed 100 kW-class tidal current turbines. *International Journal of Naval Architecture and Ocean Engineering*, 4(3), 241-255.

Appendix

In 2015 and 2016, We have conducted a series of experiments in the circulating water channel and the towing tank in the Chiba station of the University of Tokyo. It is the first time to generate shear flow in a circulating water channel and to measure out of plane bending moment at one blade root by load cells in an ocean current turbine in the shear flow.

A.1 Shear Flow Generation

The shear flow profile we designed is mainly according to the observation data in the Kuroshio Current, where the minimum speed in water depth has a 10% deduction compared with the highest flow speed in the water depth.



Fig A.1 Scene graph of the circulating water channel in Chiba station

Table A.1 Size parameters of the circulating water tank (same as Table 3.1)

Total depth	1.4m
Water depth	1.1m- 1.2m
Width	1.71m

A.1.1 Froude Similarity

Full-scale ocean current turbine has rated velocity V_a of 1.5m/s, with the diameter of blades (L_a) 40m. Considering the size and layout of the circulating water channel, shown in Fig A.1 and Table A.1, for model current turbine data, diameter of blades (L_m) is chosen as 0.88m. According to the Froude Similarity, the velocity of the experimental flow (V_m) can be calculated with following formula:

$$V_m = V_a \sqrt{\frac{L_m}{L_a}} = 0.22\text{m/s} \quad (\text{A.1})$$

When the flow speed is below 1m/s, empirically it is rather difficult to ensure the stability of the flow maker in the circulating water channel. Another reason taken into account is that the model blade is unable to bear flow speed over 0.5m/s in strength. Therefore, the designed velocity of the experimental flow (V_m) is chosen as 0.5m/s.

A.1.2 Shear Flow Generator Grid Design

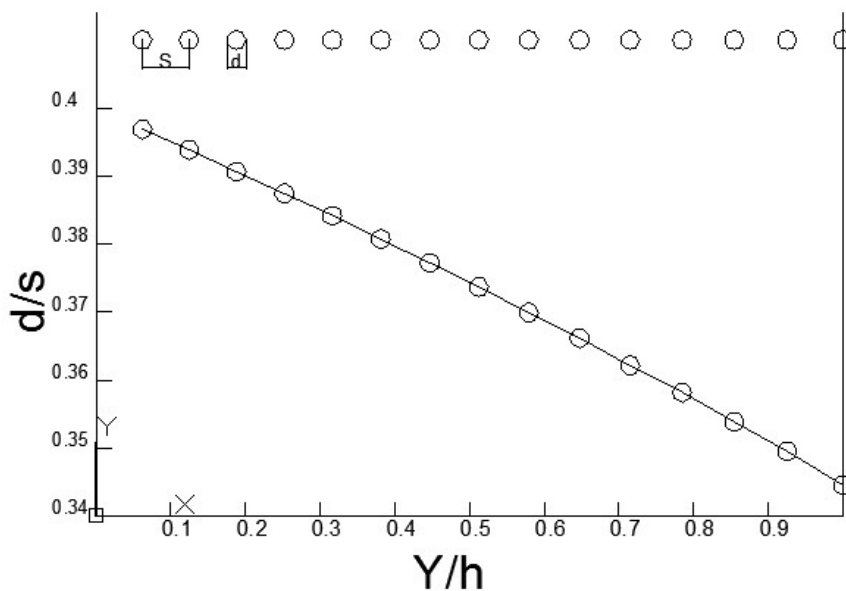


Fig A.2 Grid solidity distribution

We chose steel rods of 21.7, 27.2, 34 mm diameter according to the size of the circulating tank and the guideline of steel rods for general structure, based on the analysis by Owen & Zienkiewicz [100]. It is advised by Corrsin (1963) [103] that to use a maximum solidity less than 0.4 to minimize the instabilities and resulting non-uniformities, so we used the maximum solidity as 0.4.

As the essential characteristic of the grid used in the design, Solidity distribution is calculated using empirical equation by Rose (1965) [101] as follows,

$$\frac{\sigma_g}{(1-\sigma_g)^2} = K_0 \left(1 - \frac{2h_g\lambda}{U_\infty} \left(\frac{1}{K_0} + \frac{1}{1+a_g} \right) \left(\frac{y}{h_g} - \frac{1}{2} \right) \right) \quad (\text{A.2})$$

where, $a_g = \frac{1.1}{\sqrt{1+K_0}}$, $\lambda = \frac{\partial U_\infty}{\partial y}$, U_∞ is the free stream speed, h_g is the total height of the grid (m).

Then design values are chosen as: $K_0 = 0.9565$, $\lambda=0.1$, $\sigma_{g_{max}} = 0.4$, which are decided as recommended by Rose (1965) [101].

When the diameter of the rod is chosen as 27.2 mm, the grid solidity distribution is shown in Fig A.2. The applied distribution of rods to the experiments aimed at achieving a shear flow that has similar profile with the analysis of the ADCP measurement data. When the diameter is chosen as 27.2 mm, the expected shear flow and the plane of non-uniform grid are shown as Fig A.3 and Fig A.4.

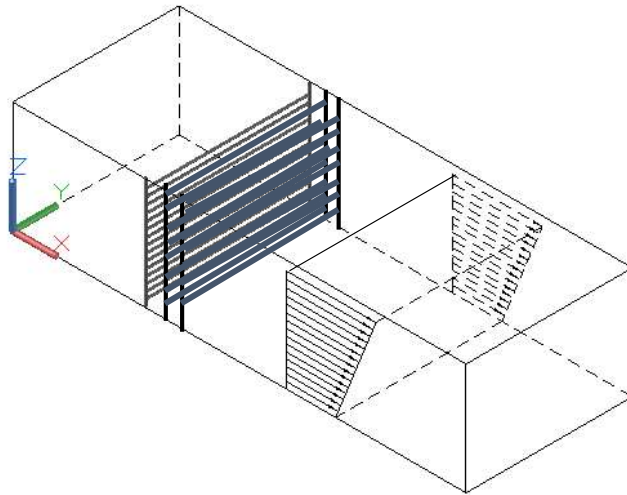


Fig A.3 Arrangement of the grid and coordinate system

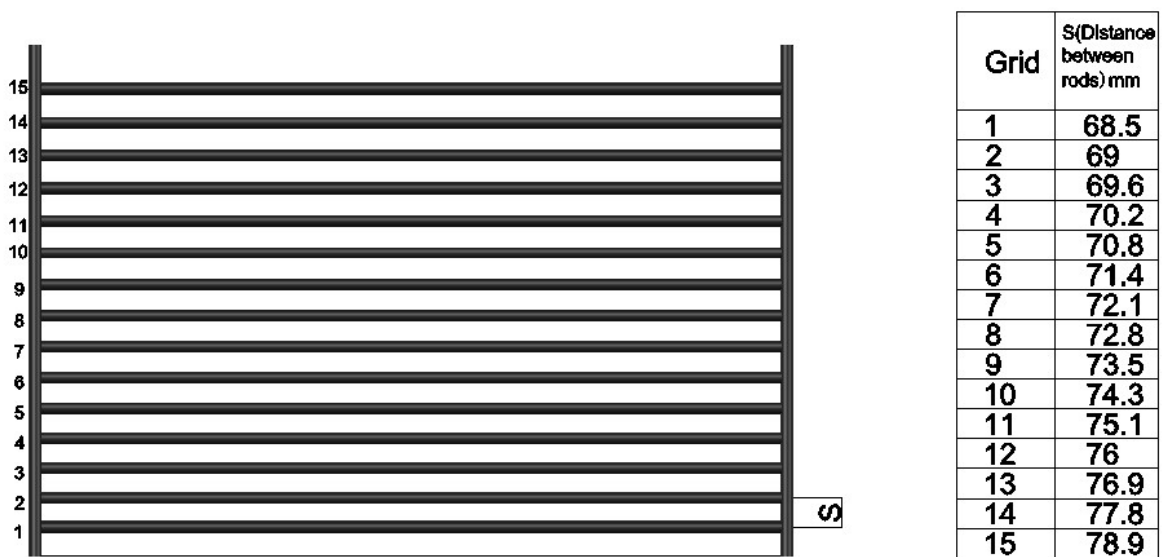


Fig A.4 Front view of the non-uniform grid

A.1.3 Strength Evaluation of Grids

The deflection and drag force of the three grids can be obtained with different steel rod diameters (Table A.2), where I is the moment of inertia of the rod in the grid (m^4). As the result is shown, the strength of all the three kinds of grid is sufficient.

Table A.2 Deflection and drag force under different grid diameters

Diameter (mm)	Thickness (mm)	I (m ⁴)	Deflection (mm)	Drag Force (N)
21.7	2.0	6.06E-09	0.07	96.14
27.2	2.0	1.26E-08	0.04	100.42
34	2.3	2.89E-08	0.02	100.42

A.1.4 Flow Measurement

Three electromagnetic current meters were used to measure the flow speed at different locations and different water depths, as shown in Fig A.5. In the experiments, a nearly linear shear flow was created by inserting 3 screens of parallel bars in the circulating water channel, the schematic diagram of the experiment is shown in Fig A.6.

Two accurate electromagnetic current meters were used to measure the centerline of the working section of the model turbine, 2 m from the location of the grids, in different water depth, also 0.2m left and 0.2m right of the centerline.

From this experiment, shear flow was obtained when three grids were placed in 2 m distance from the current meters and the averaged flow speeds by over 1 minute were about 0.42 m/s, 0.48 m/s and 0.52 m/s. The shear profile of one example shows as Fig A.7.



Fig A.5 Arrangement of electromagnetic current meters

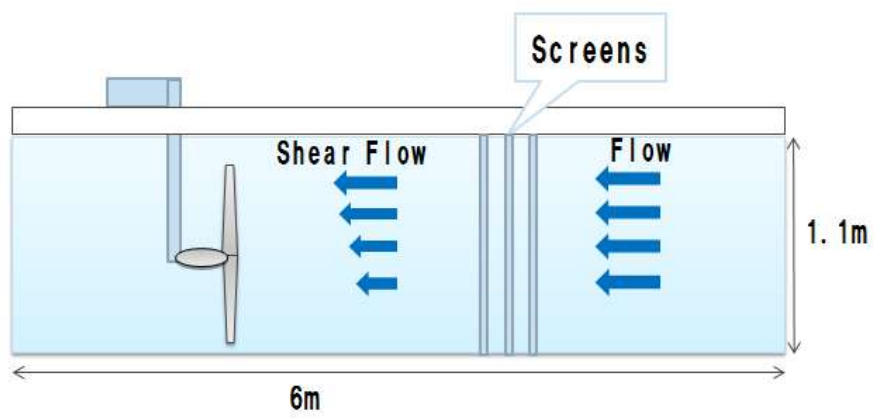


Fig A.6 Schematic of the turbine testing experiment

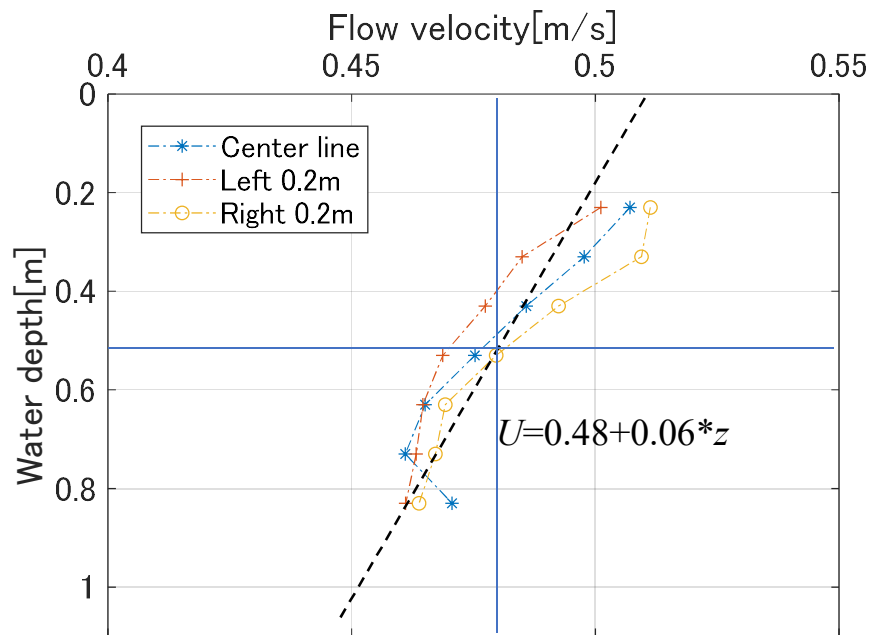


Fig A.7 Measured flow velocity with water depth (same as Fig 3.1)

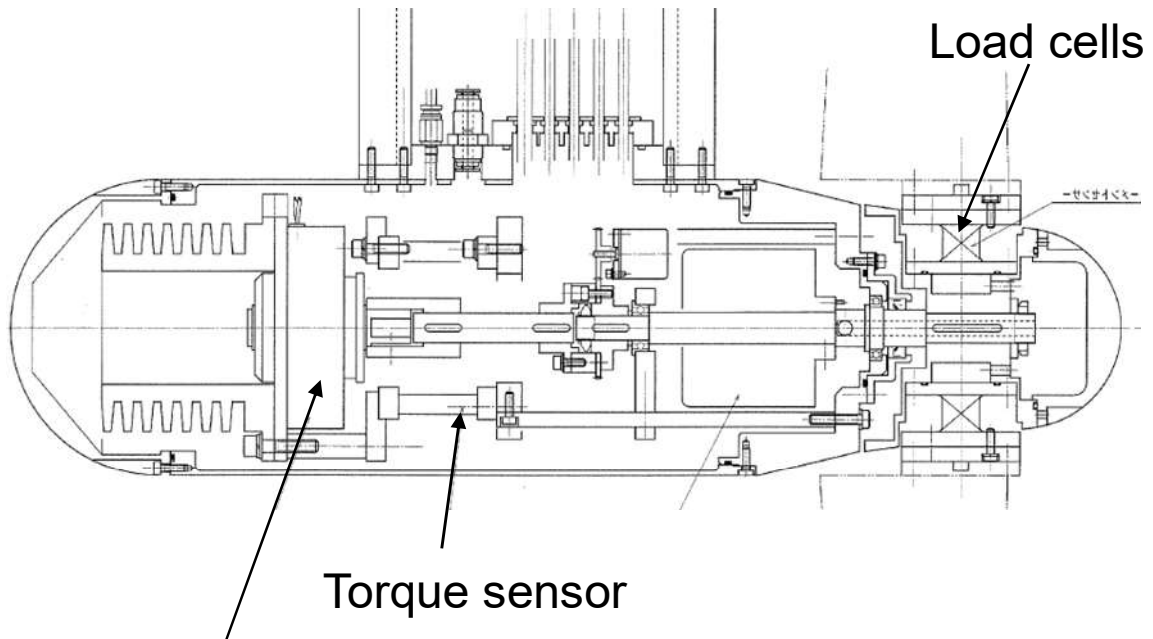
A.2 Model Turbine Test in the Circulating Water Channel

A rotor diameter of 0.88m (1/50 scale) was selected to maximize Reynolds number with low blockage ratio in the circulating water channel. The sectional shape of blades is NACA0012. The distributions of blade chord and twisting angles are presented in Table A.3. The model blades were made from aluminum for accuracy.

The rotor hub has 0.12 m diameter and has two removable bolts that fix each blade, making it possible to change the blade pitch angle. Three pitch angles, i.e. -2 degree, 0 degree and 2 degree, are adopted in the measurement. The blade twisting angles in Table A.3 refer to a pitch angle of 0°. A turbine frame that could be fixed in both the circulating water channel and the carriage of the towing tank was designed. There are load cells to measure the out of plane bending moments and in plane bending moments at one blade root. There is also a torque sensor to measure the torque. Model diagram of experimental model turbine is shown in Fig A.8.

Experiments were conducted to measure the torque and blade root bending moments of a 0.88m rotor in a circulating water channel in the Chiba experiment station of the University of Tokyo in 2015. The experimental turbine model used is shown in Fig A.9 and the whole turbine design is shown in Fig A.10. The starting time of measurement is defined as Fig A.11, when the blade of model turbine is vertical with the water level. Thus the direction of phase angle lag of the flapwise bending moment coefficient is also defined.

The Chiba circulating water channel has a working section of 1.8 m×1.1 m and the maximum flow speed is 1.3 m/s. In the circulating water channel, the turbine model is fixed in the center of the work section prior to the flow. The layout of the frame in experiment is shown in Fig A.12. These settings ensure a controlled experimental environment.



Brake system

Fig A.8 Internal layout of experimental turbine

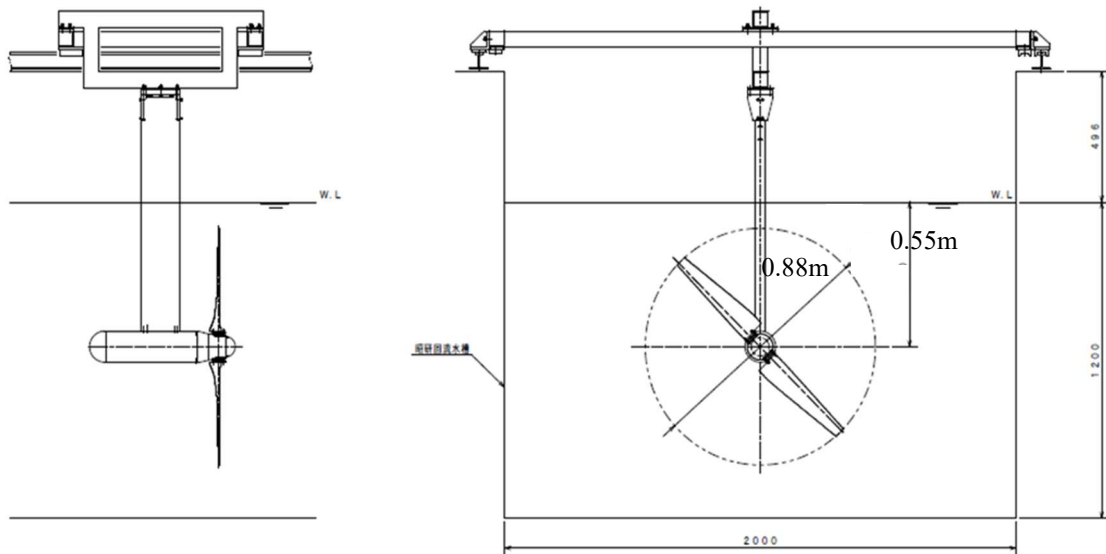


Fig A.9 Side and front view of experimental turbine (same as Fig. 3.3)



Fig A.10 1/50 scale model of two bladed horizontal axis ocean current turbine

Table A.3 Geometry of turbine blades and hub

r/R	Radius [mm]	Chord [mm]	Twisting angle [deg]
0.14	60	75.64	41.25
0.18	80	74.18	33.05
0.23	100	72.73	26.79
0.27	120	71.27	21.97
0.32	140	69.82	18.18
0.36	160	68.36	15.16
0.41	180	66.91	12.70
0.45	200	65.45	10.67
0.50	220	64.00	8.97
0.55	240	62.55	7.53
0.59	260	61.09	6.29
0.64	280	59.64	5.21
0.68	300	58.18	4.27
0.73	320	56.73	3.45
0.77	340	55.27	2.71
0.82	360	53.82	2.05
0.86	380	52.36	1.46
0.91	400	50.91	0.93
0.95	420	49.45	0.44
1.0	440	48.00	0

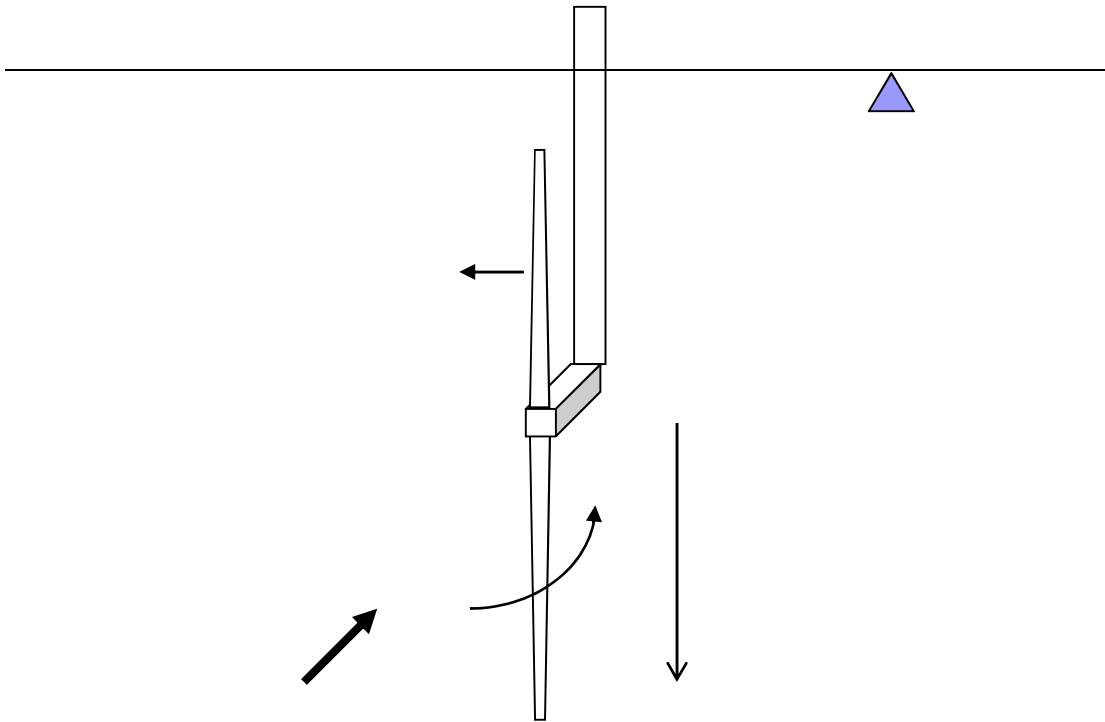


Fig A.11 Starting position of the phase angle



Fig A.12 Model turbine in the circulating water channel at 0.48 m/s

A.3 Model Turbine Test in the Towing Tank

To get accurate measurement of model turbine in uniform flow, the same model turbine was tested in the towing tank in the Chiba experimental station of the University of Tokyo in 2016. The towing tank has a length of 50 m, width of 10 m and depth of 5 m. In the towing tank, the rotor was centered at 0.2 m below the water surface. The set-up in the towing tank is shown in Fig A.13. The schematic diagram of the experiment in the towing tank is shown in Fig A.14.

The model turbine is fixed with the carriage of the towing tank, which can be moved at a constant speed. Three pitch angles, -2 degrees, 0 degree and 2 degrees are adopted in the measurement. The torque and out of plane bending moment and in plane bending moment at one blade root were measured in the same flow velocities at turbine hub center as the cases in the circulating water channel.

The objective is to correct the blockage effect of the turbine model in the circulating water tank experiment. In the experiment in the circulating water tank, the turbine projection area occupied in the cross-section of the circulating water tank (blockage rate) was as large as 29%, but in the towing tank, the blockage rate is only 1.2%, so the influence of the blockage effect is considered to be sufficiently small. As the turbine is towed at a constant speed by a carriage in still water, turbulence of inflow velocity and spatial fluctuation are also considered to be negligible.



Fig A.13 Model turbine in the towing tank

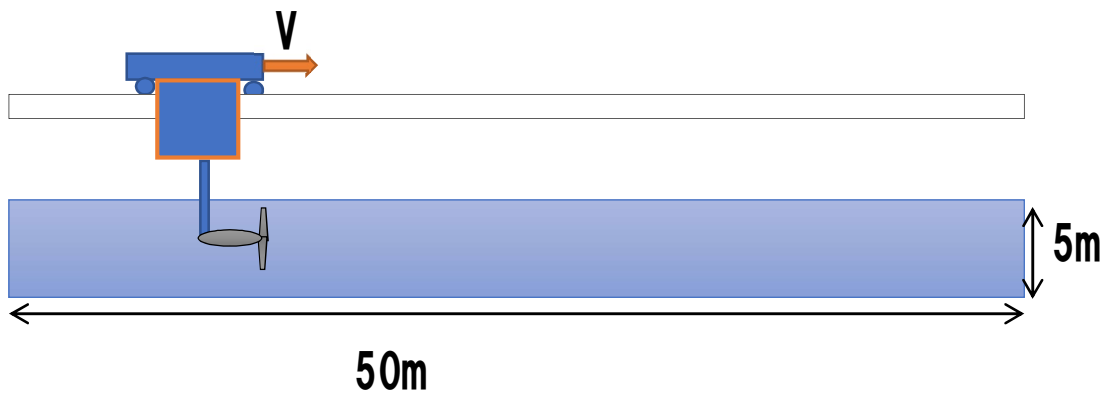


Fig A.14 Schematic diagram of the experimental arrangement in the towing tank

A.4 Analysis of Experimental Data

A.4.1 Blockage Correction

Blockage effect means that when the experimental model is placed in a flow path surrounded by the water tank, the obstruction by the model and the obstruction of the apparent flow path due to the wake will make the dynamic pressure near the model turbine increase, resulting in a larger load to be measured. In the measurement in the circulating water tank, the ratio of the projected area of the turbine to the flow area (blockage ratio) is as large as 29%, so it is considered that the load is excessively measured due to the blockage effect.

Experimental results from the circulating water channel have been corrected for blockage using the model of Ref. [56]. The flow velocity in the free flow without blockage effect is defined as U_F and the flow velocity in a channel with blockage effect is defined as U_T , then the blockage effect is corrected as following equations:

$$C_{PF} = C_{PT} \left(\frac{U_T}{U_F} \right)^3 \quad (\text{A.5})$$

$$C_{TF} = C_{TT} \left(\frac{U_T}{U_F} \right)^2 \quad (\text{A.6})$$

$$TSR_F = TSR_T \left(\frac{U_T}{U_F} \right) \quad (\text{A.7})$$

where C_{PF} is the power coefficient without blockage effect, C_{PT} is the power coefficient with blockage effect, C_{TF} is the thrust coefficient without blockage effect, C_{TT} is the thrust coefficient with blockage effect, TSR_F is the tip speed ratio without blockage effect, TSR_T is the tip speed ratio with blockage effect,

One example of blockage correction in magnitudes of power coefficients and tip speed ratios for the shear flow case are presented in Fig A.15 and Table A.4.

Table A.4 Blockage corrections for 1° pitch angle at $TSR=8$

	Circulating water channel	Towing tank
Blockage area ratio (%)	29	1.2
Reduction in C_P (%)	23	0
Reduction in TSR (%)	8.3	0
Reduction in C_{my} (%)	1.1	0

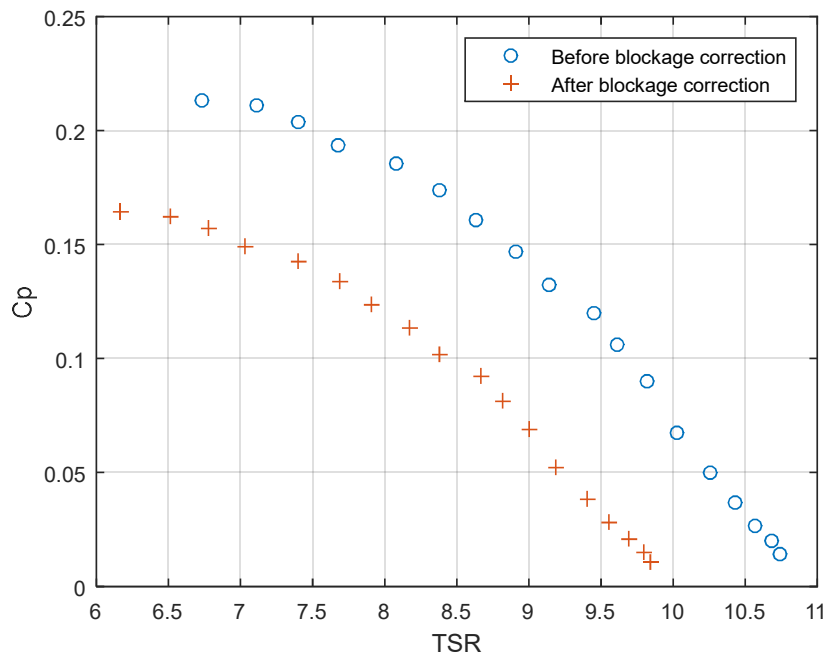


Fig A.15 Blockage corrections for 1° pitch angle

A.4.2 Analysis of Experimental Data in Frequency Domain

Using the experiment results, we checked the time history of out of plane bending moment at the blade root of ocean current turbine model in frequency domain. Power spectrum of the out of plane bending moments at one blade root shows that the frequency of the first peak agrees well with the averaged angular velocity of the ocean current turbine model, and the second peak agrees well with the second harmonic as presented in Fig A.16a. The period gram shows small peaks in the uniform flow, which is supposed to be vibrations of the equipment, since the structure of experimental setup for the turbine is not strong enough and vibrations are observed in the experiment. Another source of fluctuation could be the turbulence in the circulating water channel, but it seems negligible.

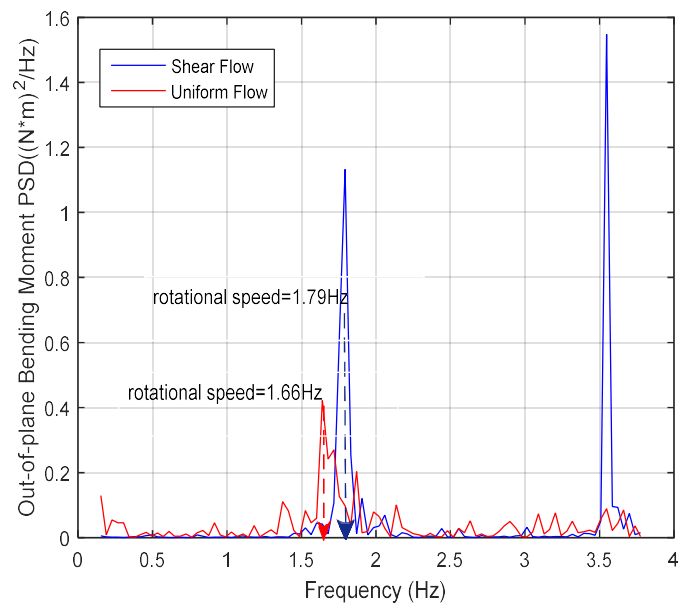


Fig A.16a Power spectrum of the out of plane bending moment at the blade root when pitch angle is 1°

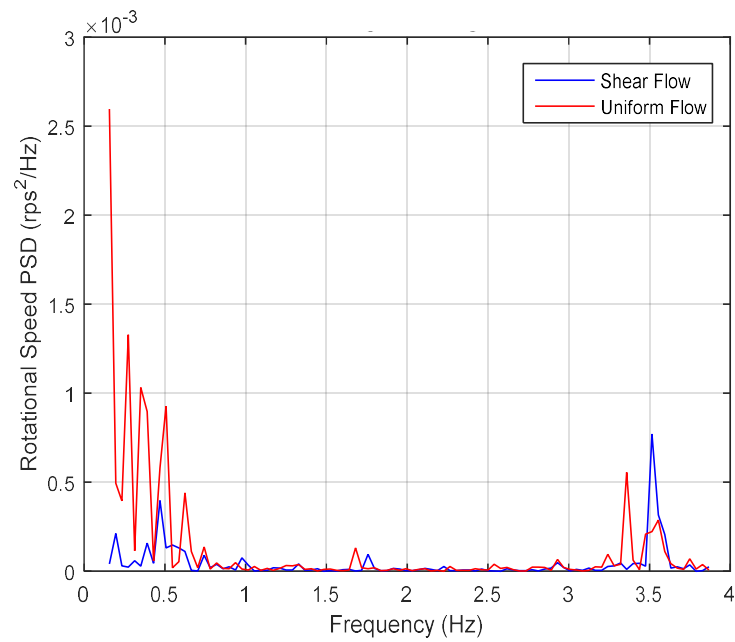


Fig A.16b Power spectrum of the angular velocity when pitch angle is 1°

The second peak of power spectrum of the angular velocity in Fig A.16b is considered to be mainly caused by the nonlinear hydrodynamic force, since the frequency corresponds to the second harmonic of the angular velocity. However, there are unexpected long-term fluctuation are observed, which is supposed to be caused by the defect of the brake system.

A.4.2 Analysis of Experimental Data in Time Domain

When analyzing the experimental values in frequency domain, we found that the angular velocity of the model turbine is not constant with time. Fig A.17a and Fig A.17b shows two examples of this measured angular velocity of the ocean current turbine rotor in time domain. The angular velocity was measured by encoders recording pulses for every circle of the blade. We used a one-second time slot to count the number of pulses, then we calculate the approximated instantaneous angular velocity of the test turbine.

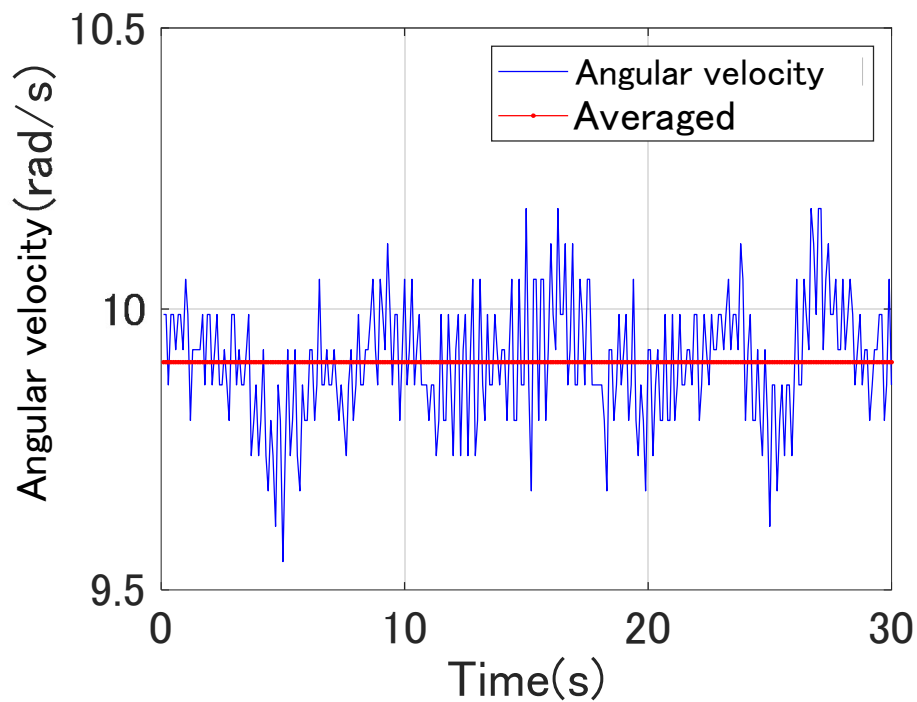


Fig A.17a Measured time history of angular velocity of the ocean current turbine rotor with the target *TSR* of 9.1

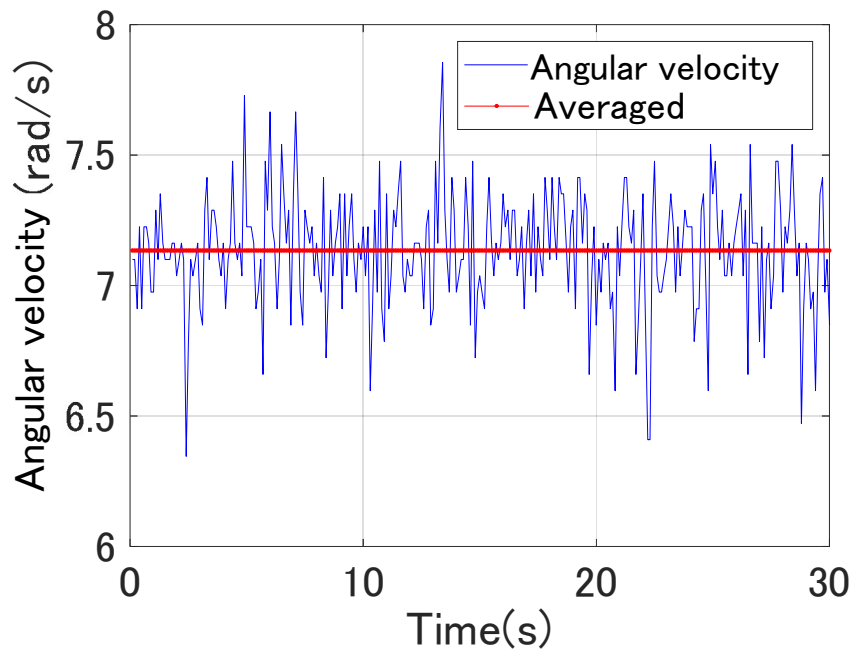


Fig A.17b Measured time history of angular velocity of the ocean current turbine rotor with the target *TSR* of 6.4

Fig A.18 shows two examples of the measured torque and in-plane bending moment at blade root (M_x), out of plane bending moment at blade root (M_y) of the ocean current turbine rotor in time domain. It shows that the fluctuation in angular velocity affects the hydrodynamic loads in time domain.

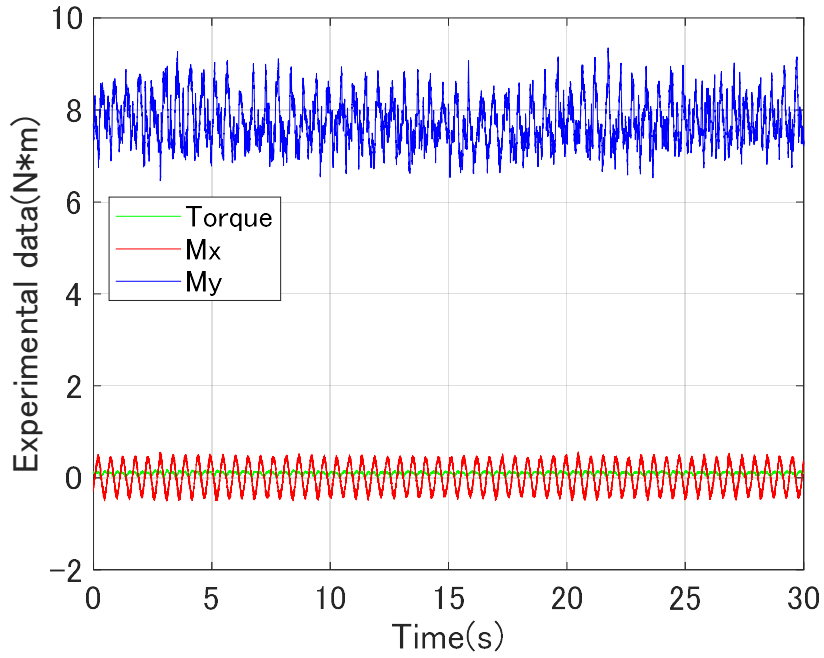


Fig A.18a Measured time histories of loads in the shear flow with target *TSR* of 9.1

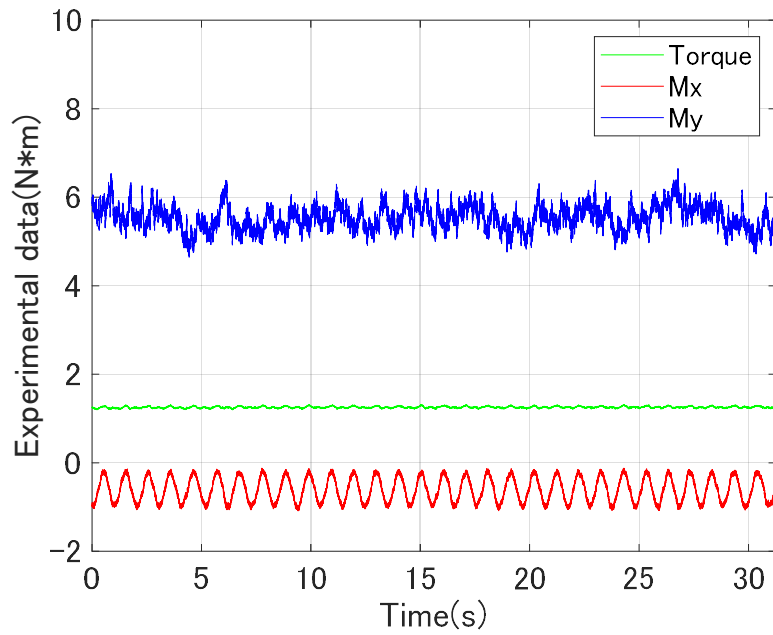


Fig A.18b Measured time histories of loads in the shear flow with target *TSR* of 6.4

A.5 Limitation of Experiments

Because of the device design and the condition of the circulating water channel, there are several limitations in the experiments.

There were unexpected low-frequency fluctuations for the load measured due to the brake system. The angular velocity of the model turbine is not constant or periodic with time. Moreover, only results at high tip speed ratios were obtained because of the unsteady behavior of the brake system when TSR is less than 6.

The power coefficient is low due to the design of the twisting angle. Comparison between BEM and the experiment will be discussed in detail in Section A.9. Also, the rotor thrust of the model turbine was not measured. Due to these limitations, based on the experiment system established in this study to generate shear flow and design test turbine model, Yahagi and Takagi[106] conducted similar experiments of generating linear shear flow, and tested the turbine with improved design in shear flow in Akishima Laboratories Inc with better facilities. For study of blockage correction, the same turbine was measured in the towing tank on the Kashiwa campus of the University of Tokyo.

Because the measured data by Yahagi are considered to be more reliable, his experimental results are used for comparison with simulation results in this study, for readers' convenience, Yahagi's experiments will be briefly introduced in Section A.6.

A.6 Experiments of Ocean Current Turbine Model

A.6.1 Turbine Tests in the Circulating Water Channel in Akishima Laboratories Inc

Using the same method to make three grids, shear flow was generated in the circulating water channel in Akishima Laboratories Inc by Yahagi et al. [104], as shown in Fig A.19.

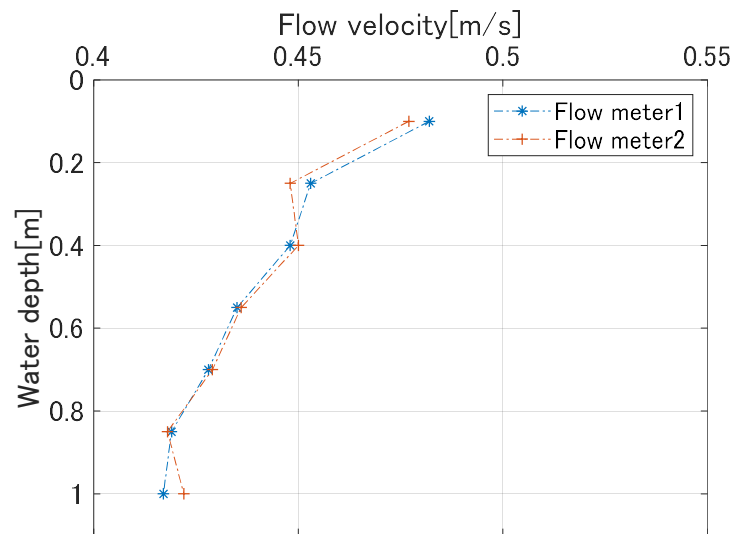


Fig A.19 Measured flow speed with water depth in Akishima Laboratories Inc.
(same as Fig 3.2)

A model turbine having angular velocity fixed with motor was designed with a diameter of 0.9m. The blade sections used the NACA0012 section. Torque, thrust and bending moments at one blade root of the ocean current turbine model were measured with pitch angle -2 degree, 0 degree and 2 degree. Fig A.20 shows schematic of the test turbine in the shear flow generated in the circulating water channel. Geometry of the turbine blade and hub is shown in Table A.5.

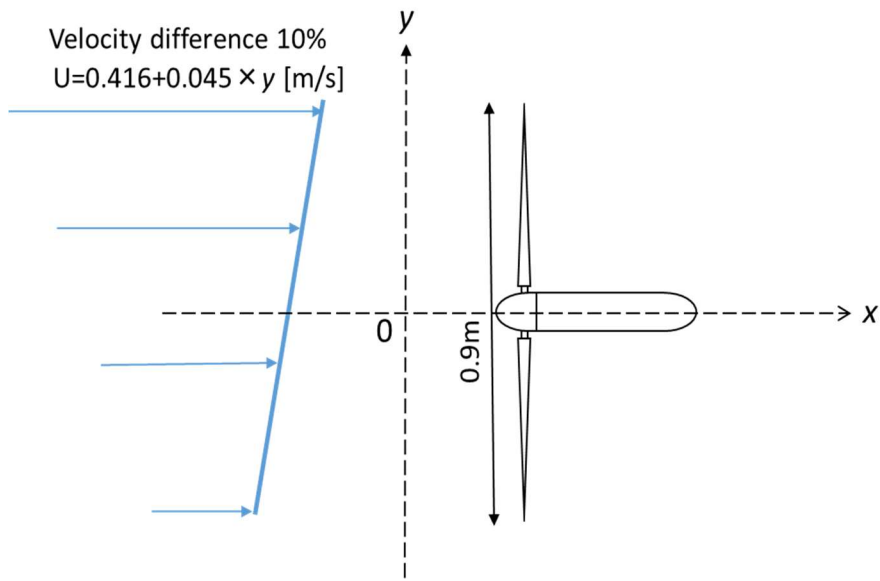


Fig A.20 Side view of the test turbine in the shear flow [106]

Table A.5 Geometry of turbine blades tested in Akishima Laboratories Inc. [104]

r/R	Radius [mm]	Chord [mm]	Twisting angle [deg]
0.13	60	100.7	29.2
0.18	80	97.5	21.8
0.22	101	94.3	16.9
0.27	121	91.1	13.4
0.32	142	87.9	10.9
0.36	163	84.7	8.9
0.41	183	81.5	7.4
0.45	204	78.3	6.2
0.50	224	75.1	5.2
0.54	245	71.9	4.3
0.59	265	68.8	3.6
0.63	286	65.6	3.0
0.68	306	62.4	2.4
0.73	327	59.2	1.9
0.77	347	56.0	1.5
0.82	368	52.8	1.2
0.86	388	49.6	0.8
0.91	409	46.4	0.5
0.95	429	43.2	0.3
1.00	450	40.0	0.0

A.6.2 Turbine Tests in the Towing Tank

Load tests of the turbine under uniform flow conditions in still water were conducted in the towing tank on the Kashiwa campus of the University of Tokyo, as shown in Fig A.21. The towing tank has a width of 10 m, a length of 50 m, and a water depth of 5 m. The experiment was conducted in September 2017 by Yahagi and Takagi [106].

The model turbine is fixed with the carriage of the towing tank, which can be moved at a constant speed. The torque, thrust and out of plane bending moment and in plane bending moment at one blade root were measured in the same averaged flow velocities with the cases in the circulating water channel.

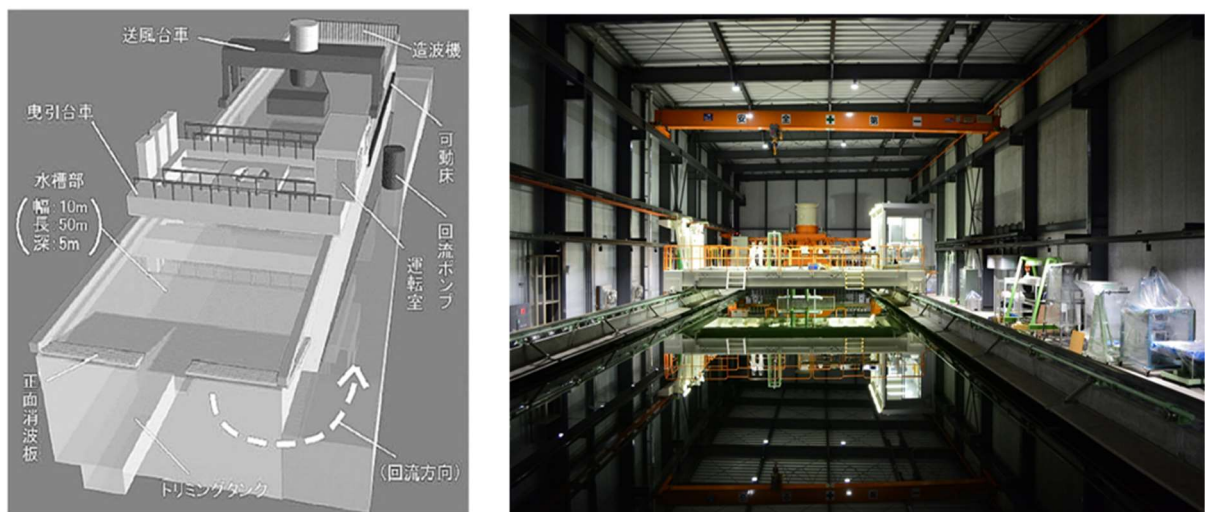


Fig A.21 Photograph of the test turbine in the towing tank [104]